Semidiscrete Galerkin Modelling of Compressible Viscous Flow Past a Circular Cone at Incidence

By

Andrew James Meade, Jr.

B.S. (Rice University) 1982
M.S. (University of California) 1984

DISSERTATION

Submitted in partial satisfaction of the requirements for the degree of

DOCTOR OF PHILOSOPHY

in

ENGINEERING
MECHANICAL ENGINEERING

in the

GRADUATE DIVISION

of the

UNIVERSITY OF CALIFORNIA at BERKELEY

Approved: Maurice Holt October 30 1989
Chair Date

Semidiscrete Galerkin Modelling of Compressible Viscous Flow Past a Circular Cone at Incidence

By

Andrew James Meade, Jr.

B.S. (Rice University) 1982
M.S. (University of California) 1984

DISSERTATION

Submitted in partial satisfaction of the requirements for the degree of

DOCTOR OF PHILOSOPHY

in

ENGINEERING
MECHANICAL ENGINEERING

in the

GRADUATE DIVISION

of the

UNIVERSITY OF CALIFORNIA at BERKELEY

Approved: Maurice Holt October 30, 1989
Chair Date

****

Semidiscrete Galerkin Modelling of Compressible Viscous Flow Past a Circular Cone at Incidence

By

Andrew J. Meade Jr.

Mechanical Engineering

Chairman, Thesis Committee

Abstract

A numerical study of the laminar and compressible boundary layer, about a circular cone in a supersonic free stream, is presented. It is thought that if accurate and efficient numerical schemes can be produced to solve the boundary layer equations, they can be joined to numerical codes that solve the inviscid outer flow. The combination of these numerical codes is competitive with the accurate, but computationally expensive, Navier-Stokes schemes.

The primary goal of this study is to develop a finite element method for the calculation of three dimensional compressible laminar boundary layer about a yawed cone. The proposed method can, in principle, be extended to apply to the three dimensional boundary layer of pointed bodies of arbitrary cross section.

In the present thesis the three dimensional boundary layer equations governing supersonic free stream flow about a cone are examined. The three dimensional partial differential equations are reduced to two dimensional integral equations by applying the Howarth, Mangler, Crocco transformations, a linear relation between viscosity, and a Blasius-type of

similarity variable. This is equivalent to a Dorodnitsyn-type formulation. The reduced equations are independent of density and curvature effects, and resemble the weak form of the two dimensional incompressible boundary layer equations in Cartesian coordinates. In addition the coordinate normal to the wall has been stretched, which reduces the gradients across the layer and provides high resolution near the surface.

Utilizing the parabolic nature of the boundary layer equations, a finite element method is applied to the Dorodnitsyn formulation. The formulation is presented in a Petrov-Galerkin finite element form and discretized across the layer using linear interpolation functions. Linear functions were chosen for ease of programming while also providing adequate accuracy. The finite element discretization yields a system of ordinary differential equations in the circumferential direction. The circumferential derivatives are solved by an implicit and noniterative finite difference marching scheme.

Solutions are presented for a 15° half angle cone at angles of attack of 5° and 10°. The numerical solutions assume a laminar boundary layer with free stream Mach number of 7. Results include circumferential distribution of skin friction and surface heat transfer, and cross flow velocity distributions across the layer.

Acknowledgement

I would like to start by thanking my research advisor, Professor Maurice Holt, for the years of patience, support, and encouragement he has given me throughout my stay at U. C. Berkeley.

I would also like to thank Professor Edmund V. Laitone and Professor Robert F. Steidel for their helpful suggestions and interest in my doctoral studies.

The helpful comments of Professor Clive A. J. Fletcher at University of Sydney, Australia, and Dr. Petrus P. van der Walt at U. C. Berkeley are gratefully acknowledged.

I would also like to acknowledge Dr. Paul Kutler and project monitor Dr. Lewis B. Schiff at the NASA Ames Research Center for the partial support through NASA Ames - UC Cooperative Agreement No. NAG-2-483.

Finally I would like to thank my family and my close friends here in the Bay Area for their love and support during my school years.

NOMENCLATURE

a	speed of sound
$b1_j, \ldots, b12_j$	nodal variables defined in equation (4.2)
C	constant defined in equation (3.7)
C_{fu}	coefficient of friction at the cone wall in the x direction
C_{fw}	coefficient of friction at the cone wall in the ϕ direction
c_p	specific heat at constant pressure
c_v	specific heat at constant volume
$C1_{kj}, \ldots, C12kj$	matrix components defined in appendix A
$D1_k, \ldots, D3_k$	vector components defined in equations (5.2a-c)
$DD1_k, \ldots, DD3_k$	vector components defined in equations (5.4a-c)
f	variable defined in equation (B.2)
g	variable defined in equation (B.2)
H	total enthalpy
$l_1, \ldots, l_{12}$	coefficients defined in equation (3.13)
$lx_1, \ldots, lx_{12}$	weighted average of $l_1, \ldots, l_{12}$ respectively
M	Mach number
N	maximum number of nodes
N_j, N_k	interpolation functions
p	pressure
$Q1_j, \ldots, Q12_j$	nodal variables defined in equation (4.4)
Q_w	heat transfer at the cone wall
$\tilde{r}$	coordinate along the cone generator
r	local radius of the cone
s	variable defined in equation (3.11)
t	time
U	velocity
u	velocity component along the cone generator
u_j	nodal value in equation (2.8)
v	velocity component normal to the surface
w	velocity component in the circumferential direction
x	coordinate along the cone generator
y	coordinate normal to the cone surface

Greek Letters

α	angle of attack; incidence
Δ	step size
Λ	variable defined in equation (B.2)
γ	specific heat ratio
ϵ	circumferential position defined in equation (5.1)
η	independent similarity variable, defined in equation (3.10)
θ	angular coordinate measured from cone axis
μ	coefficient of viscosity
ρ	density
τ	variable defined in equation (3.14)
ϕ	circumferential coordinate measured from the windward ray

Subscripts

axi	conditions obtained from the cone at zero incidence
b	conditions obtained at the cone half angle
e	conditions at the boundary layer edge
ex	exact conditions
k, j, l, m	dummy indices
s	conditions at the shock surface
w	conditions at the cone wall
0	conditions at stagnation
1	intermediate dimensionless variable
2	final dimensionless variable
∞	free stream conditions

Superscripts

n	time level or circumferential position
*	critical conditions
0	initial conditions
---	overbar indicates dimensional variable

Table of Contents

1. INTRODUCTION

The supersonic flow over sharp conical bodies at angles of attack has been a topic of considerable interest, both theoretically and experimentally, for the past three decades. This interest stems from the following properties.

(i) The geometry of conical bodies possess a high lift to drag ratio at hypersonic speeds and excellent trajectory accuracy. This makes conical bodies prime re-entry vehicles.

(ii) There is a requirement in future aircraft and missiles, which possess conical forebodies, for greater control at high angle of attack flight. The characteristics of high angle of attack flight are strong viscous-inviscid interaction and three-dimensional flow separation.

(iii) The theoretical assumption of supersonic conical flow allows for simplification in analysis while it also reveals detailed flow behavior that is typical of more complex geometries.

The theoretical investigations of the flowfield can be divided into two main classes, corresponding to the inviscid and viscous models. The viscous models require the solution of an approximation of the Navier-Stokes equations for the simulation of the flowfield. Helliwell and Lubard [1] solved the approximation of the full equations (ignoring streamwise viscous diffusion) for laminar flow about a cone, at small to moderate angles of attack. McRae and Hussaini [2] also used the same Navier-Stokes approximations to solve for both laminar and turbulent flow, at moderate incidence. Degani [3] has solved a similar set of equations for the cone at high angles of attack for turbulent flows. All of the solutions mentioned model most of the physical mechanisms and should give a more accurate prediction of the flow field than the inviscid models. However, the greatest drawback these viscous models possess, are their requirements for large amounts of computer time and storage. It is found that the inviscid models, because of their relative speed and simplicity, are still in wide use in theoretical investigations.

For inviscid analysis the flow field is considered conical. While the flow is in a real sense three-dimensional, all flow variables depend on only two coordinates θ and ϕ (Fig. 1a and b). Since the partial differential equations are nonlinear, with unknown boundary conditions at the outer shock, a numerical method must be used in order to obtain solutions. Historically the first attempt to obtain a numerical solution for the flow was made by Stone [4],[5]. Many of the inviscid models used for conical bodies make use of vortex filaments [6], point vortices [7], or the popular Euler equations. As a less expensive alternative to the Navier-Stokes equations, the Euler equations offer many attractive features. In contrast to potential methods, the Euler equations provide the correct Rankine-Hugoniot shock jump conditions, and correctly describe the transport of vorticity. The solution of the Euler equations about the cone have been made by a variety of methods. Reference [8] contains a comprehensive bibliography of the early solution schemes. The more recent methods include the popular shock-capturing [9] and finite volume schemes [10].

All of the inviscid models considered assume that viscous effects can be approximated by experiments or theoretical means. The yawed cone in supersonic flow has been studied experimentally by Holt and Blackie [11], Tracy [12], Rainbird [13], and Yahalom [14], among others. Yahalom contains an excellent bibliography of experimental studies prior to 1971. Some of the later studies include references [15],[16], and [17]. Unfortunately, experimental data are usually expensive and difficult to obtain for the conditions of interest. Moderate to high angles of attack result in flow separation from the cone, and require an interaction process between the inviscid and the significant viscous flow regions. Experimental data are not sufficient. The most straightforward and accurate means of accomplishing the interaction, requires an iterative procedure between the external flow and a theoretical viscous model.

The most familiar theoretical means of accounting for the viscous effects, is the solution of the classical boundary layer equations. The purpose of this text is to develop an accurate, computationally efficient, and general numerical scheme for the solution of the

boundary layer equations on a cone. Ultimately, it is hoped that by linking this numerical method to an efficient Euler equation solver, the resulting inviscid model can be made competitive with the existing viscous models.

An early major paper on conical boundary layers, that contains many of the ideas used in this text, is that by Moore [18]. Moore established the equations of compressible, three-dimensional boundary layer flow over a yawed circular cone. Solutions by later investigators [19]-[23], utilizing the equations of Moore, mostly used finite difference schemes, with the exception of Fletcher and Holt [24]. The latter applied an adaption of the method of integral relations (specifically the spectral method) to the governing partial differential equations, and reduced them to ordinary differential form. The method of integral relations (MIR), of reference [24], is equivalent to the method of weighted residuals (MWR) [25],[26] found in finite element literature [27],[28]. MIR permits considerably more accurate solutions to be obtained than were previously possible. However, an increase in the number of coefficients did not necessarily mean an increase in accuracy. Also, their method gives solutions up to, but not beyond, separation.

The numerical scheme presented in this text uses a combination of a Dorodnitsyn formulation of the boundary layer equations, and a finite difference/finite element procedure (semidiscrete Galerkin method) in solving the boundary layer on a yawed cone in supersonic flow.

The application of MWR, and the various transformations presented in this text, results in a Dorodnitsyn formulation of the boundary layer equations for the cone [29],[30]. This formulation is known to obtain relatively accurate solutions with only a few coefficients defining the dependent variables across the boundary layer. The high accuracy in this formulation comes, in part, from the use of the streamwise velocity component u. This transformation, in effect, acts as a stretched surface normal coordinate. The new independent variable, u, minimizes the normal gradients and provides high resolution near the wall. In addition the boundary layer equations are reduced to a set of ordinary

differential equations.

The finite element method uses piecewise continous polynomials to model dependent variables and averages out the approximation errors across the elements. This averaging allows considerable accuracy for a small number of elements. Greater accuracy can be obtained by simply increasing the number of elements. Since the boundary layer equations for the cone are parabolic, the circumferential dependence of the variables can be modelled by an implicit finite difference marching scheme. The surface normal dependence of the variables is modelled by one-dimensional elements. This arrangement is much more computationally efficient than that using two dimensional elements, and easier to program. In the past, two-dimensional boundary layer flows have been computed effectively with finite element formulations [31],[32]. However, the previous formulations have never been applied to the cone problem, nor taken full advantage of the various transformations to be found in this text.

The semidiscrete Galerkin method can be applied to cones with more general cross sections without modification. The influence of the cross section appear only through the external flow parameters that are found in equation (3.13). The method also possesses the potential capability of calculating solutions beyond flow separation.

The present studies are restricted to attached, inviscid supersonic external flow at moderate angles of attack. The boundary layer is assumed laminar and the fluid is assumed ideal with a specific heat ratio of 1.4 (air). The only geometry considered is that for a circular cone.

In chapter 2 the semidiscrete Galerkin method is explained and demonstrated, using a one-dimensional parabolic equation. Chapter 3 describes the equations of motion used in the inviscid and viscous regions, and boundary and initial conditions used for the cone. In chapter 4 the method of weighted residuals, and the semidiscrete Galerkin method in particular, is applied to the boundary layer equations. Chapter 5 presents the details of the numerical methods used to solve the equations given in chapter 4. Chapter 6 gives the

numerical results and includes the convergence curves, circumferential distribution of skin friction and surface heat transfer, and cross flow velocity distributions. Chapter 7 presents the summary of the text and the work in progress.

2. THE GALERKIN FINITE ELEMENT METHOD

The finite element method is an approximate method of solving a wide range of boundary and initial value problems. Since there are, of course, various comprehensive references on the subject of finite elements [33]-[41] this chapter will only supply sufficient background and touch on the points needed to illustrate the method, as it will be applied to the cone problem.

2.1 The Method of Weighted Residuals

Among the more popular methods in the numerical solution of fluid dynamics problems are finite difference, variational methods and the methods of weighted residuals [26]. This large class of methods can be described in the following manner. Using linear operators, it is assumed that an approximate solution to a differential equation

$$L(u) = 0 \tag{2.1}$$

is to be found subject to the boundary conditions

$$B(u) = 0 \tag{2.2}$$

and the initial conditions

$$I(u) = 0 \tag{2.3}$$

An approximate solution to u is introduced.

$$u_a(x,t) = u^0(x,t) + \sum_{j=1}^{N} N_j(x) a_j(t), \tag{2.4}$$

where $a_j(t)$ are unknowns, $N_j(x)$ are known analytic functions (trial functions), and $u^0(x,t)$ is chosen to satisfy all global boundary conditions (2.2) and initial conditions (2.3). Substitution of the approximate solution into (2.1) gives an error (residual), R. To determine the values of a_j, an inner product of the residual R and a set of linearly independent weighting

functions w_k ($k = 1, \ldots, N$) is constructed and set equal to zero.

$$\int_D w_k R \, dx = 0 \tag{2.5}$$

where D is the domain of interest.

This resembles the weak form of (2.1). As equation (2.5) is written equation (2.1) becomes a system of N ordinary differential equations in t. If the residual R is considered continuous, then as $N \rightarrow \infty$, R should converge to zero in the mean. This implies that if the approximate solution u_a satisfies the boundary conditions exactly then u_a should converge to the exact solution u in the mean. In short, by setting the inner product to zero, the errors introduced by u_a are averaged out over the domain of interest.

The choice of the weighting function determines the various subclasses to be employed. The more popular subclasses are the least squares method, the method of moments, the collocation method, the subdomain method, and the Galerkin method.

2.2 The Petrov-Galerkin Method

Basically for the subclass of Petrov-Galerkin methods [42] the weighting function is written as

$$w_k = P_k(x) \tag{2.6}$$

where $P_k(x)$ is similar to the trial function $N_j(x)$ used in u_a, but with some modifications used to satisfy requirements on the solution. The classical Galerkin method [43] uses only the trial functions for weighting. Classical Galerkin methods can be thought of as a simplified form of the Petrov-Galerkin method. To simplify matters the Petrov-Galerkin method will be referred to as the Galerkin method in this text.

To ensure that linearly independent equations exist for the solution of the values a_j,

the trial functions $N_j(x)$ and thus the weight functions must be linearly independent.

The choice of the trial functions to be used forms the two main branches known as the spectral method and the Galerkin finite element method.

2.3 The Semidiscrete Galerkin Method

The most popular branch of the Galerkin method is the Galerkin finite element method. Its popularity comes from the ease in which it can be applied to nonstructural problems. Basically the method uses low order polynomials as interpolation and weighting functions and then applies the Galerkin method within the subdomains (finite elements) formed from the domain of interest.

The semidiscrete Galerkin method [28] uses finite element representation only for spatial variation. The time derivative is replaced by some finite difference operator.

To illustrate the method and its properties, as it was applied to the cone problem, we will consider the one-dimensional unsteady heat conduction problem in nondimensional form.

$$\frac{\partial u}{\partial t} - \frac{\partial^2 u}{\partial x^2} = 0 \tag{2.7}$$

for

$$0 \le x \le 1$$

where u(x,t) represents the nondimensional temperature. The initial and boundary conditions are

$$u(x,0) = u^0(x)$$
$$u(0,t) = 0$$
$$u(1,t) = 1$$

The domain of interest ($0 \le x \le 1$) is divided into subdomains known as finite elements. As seen in figure 2 the nodal points are the element boundaries, using the variable x_j to mark the position of the nodes. The approximate solution for u is

$$u_a(x,t) = \sum_j^N N_j u_j \tag{2.8a}$$

and for u^0

$$u_a^0(x) = \sum_j^N N_j u_j^0, \tag{2.8b}$$

where N_j is the interpolation function, and u_j and u_j^0 are the values of u and u^0 respectively at the nodes. Using the interpolation function as the weighting function , N_k , and taking the weak form of (2.7) we have

$$\int_0^1 N_k \frac{\partial u_a}{\partial t}\, dx - \int_0^1 N_k \frac{\partial^2 u_a}{\partial x^2}\, dx = 0 \tag{2.9}$$

As it stands the term $\frac{\partial^2 u_a}{\partial x^2}$ cannot be represented properly. The finite element method requires that the interpolation used should provide interelement continuity of derivatives of degree one less than the maximum that appears in the weak form of the equation of interest. Piecewise continuous polynomials provide continuity for only the value u_a across the elements. Also, if at all possible, we would like to employ linear interpolation functions. If these simple functions can be shown to be completely satisfactory, there are no compelling reasons to use complicated, and numerically costly, higher order functions. Linear interpolation provides continuity within the element for only a first order derivative.

The order of the derivative can be reduced by applying the Green-Gauss theorem to the second integral. In one dimension the Green-Gauss theorem manifests itself as integration by parts. Equation (2.9) becomes

$$\int_0^1 N_k \frac{\partial u_a}{\partial t} dx = -\int_0^1 \frac{dN_k}{dx} \frac{\partial u_a}{\partial x} dx + N_k \frac{\partial u_a}{\partial x}\Bigg|_0^1 \tag{2.10}$$

The resulting boundary term is known as the natural boundary condition. If the example were of Neumann type the boundary term would be replaced by the given boundary condition. Since the example is of Dirichlet type the natural boundary condition has been incorporated into the governing equation. Using the full representation of u_a (2.8a) in equation (2.10) results in

$$\sum_j^N C1_{kj} \frac{du_j}{dt} = -\sum_j^N C2_{kj} u_j + \sum_j^N N_k \frac{dN_j}{dx} u_j \tag{2.11}$$

where

$$C1_{kj} = \int_0^1 N_k N_j \, dx$$

$$C2_{kj} = \int_0^1 \frac{dN_k}{dx} \frac{dN_j}{dx} \, dx$$

The semidiscrete Galerkin method has reduced the partial differential equation (2.7), in x and t, to a system of first order ordinary differential equtions in t. Using piecewise continuous polynomial interpolation functions, the resulting equations will be linearly independent for all N. In addition, if low order polynomials are used the integrands of the equations will also be low order polynomials, which can be solved exactly and efficiently by low order Gaussian quadrature [44]. Notice that the integrals are independent of t. If a uniform grid is used for x the values of $C1_{kj}$ and $C2_{kj}$ are constant.

For linear interpolation functions at x_j (Fig. 3)

in element A, $\quad N_j = \dfrac{x - x_{j-1}}{x_j - x_{j-1}}$,

in element B, $N_j = \dfrac{x_{j+1} - x}{x_{j+1} - x_j}$,

for $x < x_{j-1}$ $N_j = 0$

for $x > x_{j+1}$ $N_j = 0$

At a specific node x_k, the only nonzero contributions in the integrals come from the neighboring nodes, x_{k-1} and x_{k+1}, and the node itself x_k. Therefore $C1_{kj}$ and $C2_{kj}$ form tri-diagonal matrices.

The boundary term becomes

$$u_1 = 0 \qquad (2.12)$$
$$u_N = 1$$

Equation (2.11) becomes

$$\sum_j^N C1_{kj} \frac{du_j}{dt} = -\sum_j^N SC2_{kj} u_j \qquad k = 1, \ldots, N \qquad (2.13)$$

where $C2_{kj}$ has been modified to absorb the natural boundary terms and renamed $SC2_{kj}$.

The essential boundary conditions of equation (2.12) reduce the N×N arrays, $C1_{kj}$ and $SC2_{kj}$, into (N−2)×(N−2) matrices.

The ordinary differential equation is solved by introducing a discretized time domain consisting of n number of time increments, Δt. The time derivative is replaced by the finite difference form

$$\frac{u_j^{n+1} - u_j^n}{\Delta t} = \frac{\Delta u_j^{n+1}}{\Delta t} \qquad (2.14)$$

where the superscript indicates the time level. The variable Δu_j^{n+1} is solved using the theta

method [45] for integration.

$$\sum_{j}^{N} C1_{kj}\Delta u_j^{n+1} = -\Delta t(\theta \sum_{j}^{N} SC2_{kj}u_j^{n+1} + (1-\theta)\sum_{j}^{N} SC2_{kj}u_j^{n}) \tag{2.15}$$

where θ controls the degree of implicitness. The value of $\theta = 0$ gives the explicit Euler forward difference scheme, while $\theta = 1$ gives the fully implicit backward Euler difference scheme. By setting $\theta = 0.5$ the second order accurate Crank-Nicholson [45] scheme can be used.

Since the governing equation is linear, it can be simply rewritten as

$$\sum_{j}^{N} (C1_{kj} + \theta \Delta t SC2_{kj})\Delta u_j^{n+1} = -\Delta t \sum_{j}^{N} SC2_{kj}u_j^{n} \tag{2.16}$$

For a chosen Δt the right hand side term is known and forms a vector of length N−2. The array $C1_{kj} + \theta \Delta t SC2_{kj}$ is a (N−2)×(N−2) tridiagonal matrix that can be solved quite efficiently by the Thomas algorithm [46]. The Thomas algorithm factorizes the tridiagonal matrix in O(N) operations as opposed to the $O(N^2)$ operations required by Gaussian elimination [47].

To integrate in t, Δu_j^{n+1} is solved for and added to the known value u_j^n to give u_j^{n+1}. The u_j^{n+1} is then used in the right side to solve for the next time level. Notice that by varying the time step for required accuracy, iteration is not needed. This results in a computationally efficient integration algorithm.

To summarize, the application of the semidiscrete Galerkin method with the theta method for temporal integration, and the Thomas algorithm for matrix solution, makes for a very efficient computational solution of a parabolic problem.

3. GOVERNING EQUATIONS

From a computational point of view it is more practical and convenient to classify the flow about the cone into two regions, the inviscid and viscous. One may then exploit the character of the respective regions and use efficient numerical methods in their solution.

3.1. Inviscid Flow

3.1.1. Equations of Motion

In this present study the flow outside the boundary layer is assumed to be steady, supersonic and attached. The resulting main shock is assumed attached to the apex of the cone. The fluid is assumed to be inviscid and non-conducting. A spherical coordinate system is used with $\bar{r}$ measured from the cone apex, θ measured from the cone axis, and ϕ measured from the windward line of symmetry (Fig. 1a, b). The dependent variables are nondimensionalized in the following manner,

$$u = \frac{\bar{u}}{a^*} \qquad \rho = \frac{\bar{\rho}}{\rho_\infty} \tag{3.1}$$

$$v = \frac{\bar{v}}{a^*} \qquad p = \frac{\bar{p}}{\rho_\infty a^{*2}}$$

$$w = \frac{\bar{w}}{a^*} \qquad a = \frac{\bar{a}}{a^*},$$

where $\bar{a}$ is the local speed of sound and a^* is the critical speed of sound. The nondimensional form of the equations of motion for this flow are as follows.

Conservation of mass:

$$\frac{\partial v}{\partial \theta} + \frac{1}{\sin\theta}\frac{\partial w}{\partial \phi} + \frac{v}{\rho}\frac{\partial \rho}{\partial \theta} + \frac{w}{\rho\sin\theta}\frac{\partial \rho}{\partial \phi} + 2u + v\cot\theta = 0 \tag{3.2a}$$

Conservation of $\tilde{r}$ momentum:

$$v\frac{\partial u}{\partial \theta} + \frac{w}{\sin\theta}\frac{\partial u}{\partial \phi} - (v^2 + w^2) = 0 \tag{3.2b}$$

Conservation of θ momentum:

$$v\frac{\partial v}{\partial \theta} + \frac{w}{\sin\theta}\frac{\partial v}{\partial \phi} + \frac{1}{\rho}\frac{\partial p}{\partial \theta} + uv - w^2\cot\theta = 0 \tag{3.2c}$$

Conservation of ϕ momentum:

$$v\frac{\partial w}{\partial \theta} + \frac{w}{\sin\theta}\frac{\partial w}{\partial \phi} + \frac{1}{\rho\sin\theta}\frac{\partial p}{\partial \phi} + uw + vw\cot\theta = 0 \tag{3.2d}$$

Conservation of energy:

$$v\frac{\partial p}{\partial \theta} + \frac{w}{\sin\theta}\frac{\partial p}{\partial \phi} - a^2\left[v\frac{\partial \rho}{\partial \theta} + \frac{w}{\sin\theta}\frac{\partial \rho}{\partial \phi}\right] = 0 \tag{3.2e}$$

Note that since the main shock is attached (Fig. 1a,b), the dependent variables are independent of the $\tilde{r}$ coordinate.

3.1.2. Boundary Conditions

The external flow field is bounded by the body, the main shock, and the windward and leeward planes of symmetry (ϕ = 0° and 180° respectively), where the following boundary conditions are satisfied.

At each plane of symmetry:

$$\frac{\partial u}{\partial \phi}=0 \qquad \frac{\partial \rho}{\partial \phi}=0 \tag{3.3}$$
$$\frac{\partial v}{\partial \phi}=0 \qquad \frac{\partial p}{\partial \phi}=0$$
$$w=0$$
$$\frac{\partial w}{\partial \theta}=0$$
$$\frac{\partial \theta_s}{\partial \phi}=0$$

At the cone surface $\theta = \theta_b$:

$$u=u_e \qquad p=p_e \tag{3.4}$$
$$w=w_e \qquad \frac{\partial p}{\partial \phi}=\frac{\partial p_e}{\partial \phi}$$
$$v=0 \qquad \frac{\partial v}{\partial \phi}=0$$

At the main shock the conditions are given in terms of the free stream conditions and the shock slope, $\frac{\partial \theta_s}{\partial \phi}$, by the Rankine-Hugoniot relations [8].

3.2. Viscous Flow

3.2.1. Equations of Motion

The viscous flow region, prior to separation from the body, is assumed to extend over a small distance normal to the cone body. The equations of motion for viscous, laminar, compressible, and nonisentropic flow about an inclined, axisymmetric, three dimensional body are nondimensionalized. The independent and dependent variables are written in terms

of the orthogonal coordinate system shown in (Fig. 1a,b). The Prandtl boundary layer assumptions are then applied to give the resulting equations of motion [18]. The Prandtl number (Pr) is assumed constant as are the specific heats c_v and c_p.

Conservation of mass:

$$\frac{\partial}{\partial x}\left(\rho u r\right) + \frac{\partial}{\partial y}\left(\rho v r\right) + \frac{1}{r}\frac{\partial}{\partial \phi}\left(\rho w r\right) = 0 \tag{3.5a}$$

Conservation of x momentum:

$$\rho u\frac{\partial u}{\partial x} + \rho v\frac{\partial u}{\partial y} + \frac{\rho w}{r}\frac{\partial u}{\partial \phi} - \rho\frac{w^2}{r}\frac{dr}{dx} = -\frac{\partial p_e}{\partial x} + \frac{\partial}{\partial y}\left(\mu\frac{\partial u}{\partial y}\right) \tag{3.5b}$$

Conservation of ϕ momentum:

$$\rho u\frac{\partial w}{\partial x} + \rho v\frac{\partial w}{\partial y} + \frac{\rho w}{r}\frac{\partial w}{\partial \phi} + \rho\frac{uw}{r}\frac{dr}{dx} = -\frac{1}{r}\frac{\partial p_e}{\partial \phi} + \frac{\partial}{\partial y}\left(\mu\frac{\partial w}{\partial y}\right) \tag{3.5c}$$

Conservation of energy:

$$\rho u\frac{\partial H}{\partial x} + \rho v\frac{\partial H}{\partial y} + \frac{\rho w}{r}\frac{\partial H}{\partial \phi} = \frac{1}{Pr}\frac{\partial}{\partial y}\left(\mu\frac{\partial H}{\partial y}\right) + \left(1-\frac{1}{Pr}\right)\frac{\partial}{\partial y}\left(\mu\frac{\partial}{\partial y}\left(\frac{\left(u^2+w^2\right)}{2}\right)\right) \tag{3.5d}$$

The velocities are nondimensionalized in the same manner as that used in the inviscid equations of motion. Additional nondimensional variables are defined in the following manner.

$$r = \frac{\bar{r}}{L} \qquad p_\infty = \frac{\overline{p_\infty}}{\rho_\infty a^{*2}}$$

$$x = \frac{\bar{x}}{L} \qquad U_\infty = \frac{\overline{U_\infty}}{a^*} \tag{3.6}$$

$$y = \frac{\bar{y}}{L}$$

$$H = \frac{c_p T + \tfrac{1}{2}\left(\bar{u}^2 + \bar{w}^2\right)}{a^{*2}}$$

$$\mu = \frac{\bar{\mu}}{\rho_\infty a^* L},$$

where H is the total (stagnation) enthalpy.

Equations (3.5a-d) can be simplified further. These governing equations of motion are three dimensional and include variable density, an explicit dependence on the local radius r, and severe gradients normal to the wall. By various transformations these effects can be eliminated or minimized in the equations [18],[48],[49].

It is assumed that the variation of viscosity across the boundary layer can be represented by a linear relation. The viscosity μ is replaced as follows.

$$\frac{\bar{\mu}}{\overline{\mu_\infty}} = \frac{\mu}{\mu_\infty} = C\frac{T}{T_\infty}, \tag{3.7}$$

where C is some constant value. A full explanation of the equation is given by Chapman and Rubesin [50].

To remove the explicit dependence of the density we employ the Howarth transformation.

$$x_1 = x, \qquad y_1 = \left(\frac{p_\infty}{p_e}\right)^{1/2} \int_0^y \rho dy \tag{3.8}$$

To reduce the effect of body curvature (r), the Mangler transformation is used.

$$x_2 = \int_0^{x_1} r^2 dx_1, \qquad y_2 = r y_1 \tag{3.9}$$

This transformation also relates axially symmetric flow to plane flow.

The transformed equations, at this point, resemble the equations of motion for incompressible flow in three dimensional Cartesian coordinates.

We will further exploit the character of the equations in their simplified form. The outer edge of the boundary layer grows in a parabolic manner in the x direction ($y_2 \approx x_2^{1/2}$). A similarity variable can therefore be constructed.

$$\eta = \left(\frac{U_\infty}{2\mu_\infty}\right)^{1/2} \frac{y_2}{x_2^{1/2}} \tag{3.10}$$

The Blasius-type of transformation reduces the number of independent variables from three to two.

The equations of motion are simplified further still. The dependent variables u, w, H, and v are replaced by u_2, w_2, s, and v_2, respectively. They are defined as follows.

$$u_2 = \frac{u}{u_e} \tag{3.11}$$

$$w_2 = \frac{w}{u_e}$$

$$s = 1 - \frac{2H(\gamma - 1)}{(\gamma + 1)}$$

$$v_2 = \frac{1}{u_e}\left(\frac{3Re_r p_\infty}{2p_e \sin\theta_b}\right)^{1/2}\left(\rho v + u\int_0^y \frac{\partial \rho}{\partial x}dy + \frac{w}{r}\int_0^y \frac{\partial \rho}{\partial \phi}dy\right)$$

$$- \frac{\eta}{2}\left(u_2 + \frac{w_2}{p_e \sin\theta_b}\frac{\partial p_e}{\partial \phi}\right),$$

where $Re_r = \dfrac{U_\infty r}{\mu_\infty}$

The results of our various transformations and substitutions are equations (3.12a-d).

Conservation of mass:

$$\frac{1}{\sin\theta_b}\frac{\partial w_2}{\partial \phi} + \frac{\partial v_2}{\partial \eta} = l_5 w_2 - 1.5u_2 \tag{3.12a}$$

Conservation of x momentum:

$$\frac{w_2}{\sin\theta_b}\frac{\partial u_2}{\partial \phi} + v_2\frac{\partial u_2}{\partial \eta} = l_2\frac{\partial^2 u_2}{\partial \eta^2} - l_1 w_2 u_2 + w_2^2 \tag{3.12b}$$

Conservation of ϕ momentum:

$$\frac{w_2}{\sin\theta_b}\frac{\partial w_2}{\partial \phi} + v_2\frac{\partial w_2}{\partial \eta} = l_{11}(1 - s) + l_8 u_2^2 + l_8 w_2^2 + l_2\frac{\partial^2 w_2}{\partial \eta^2} - l_1 w_2^2 - w_2 u_2 \tag{3.12c}$$

Conservation of energy:

$$\frac{w_2}{\sin\theta_b}\frac{\partial s}{\partial \phi} + v_2\frac{\partial s}{\partial \eta} = l_3\frac{\partial^2 s}{\partial \eta^2} + \frac{l_4}{2}\frac{\partial^2}{\partial \eta^2}(u_2^2) + \frac{l_4}{2}\frac{\partial^2}{\partial \eta^2}(w_2^2) \tag{3.12d}$$

The simplification of the equations of motion is now complete. The four partial differential equations describing three-dimensional, viscous, compressible boundary layer, with explicit dependence on curvature, has been converted into a system of equations resembling the boundary-layer equations for two-dimensional incompressible flow in Cartesian coordinates.

The coefficients $l_1, \ldots, l_{12}$ are functions of the freestream conditions and the circumferential position ϕ. The coefficients are defined below.

$$l_1 = \frac{1}{u_e \sin\theta_b}\frac{\partial u_e}{\partial \phi} = \frac{w_e}{u_e} \tag{3.13}$$

$$l_2 = \frac{1.5C}{u_e\left(\frac{(\gamma-1)}{(\gamma+1)} + \frac{2}{(\gamma+1)M_\infty^2}\right)^{1/2}}$$

$$l_3 = \frac{l_2}{Pr}$$

$$l_4 = 2u_e^2\frac{(\gamma-1)}{(\gamma+1)}\left(\frac{1}{Pr} - 1\right) l_2$$

$$l_5 = -\left(\frac{1}{2p_e\sin\theta_b}\frac{\partial p_e}{\partial \phi} + \frac{w_e}{u_e}\right)$$

$$l_6 = -\frac{(\gamma-1)}{\gamma p_e \sin\theta_b}\frac{\partial p_e}{\partial \phi}$$

$$l_7 = -\left(\frac{1}{2\gamma p_e \sin\theta_b} \frac{\partial p_e}{\partial \phi} + 2\frac{w_e}{u_e} \right)$$

$$l_8 = \frac{(\gamma-1)}{2\gamma p_e \sin\theta_b} \frac{\partial p_e}{\partial \phi}$$

$$l_9 = -\frac{(\gamma+1)}{2\gamma u_e^2 p_e \sin\theta_b} \frac{\partial^2 p_e}{\partial \phi^2}$$

$$l_{10} = \frac{(\gamma-1)}{2\gamma p_e \sin\theta_b} \frac{\partial^2 p_e}{\partial \phi^2}$$

$$l_{11} = \frac{(\gamma+1) l_6}{2(\gamma-1)u_e^2}$$

$$l_{12} = \frac{1}{u_e \sin\theta_b} \frac{\partial w_e}{\partial \phi}$$

Using the results from the previous chapter on the method of weighted residuals we will transform the equations 3.12a-d from their differential form to an integral form. The Crocco transformation (3.14) will be applied to the integral equations to change the independent variables from ϕ and η to ϕ and u_2.

$$u_2 = \int_0^{\eta} \tau \, d\eta \tag{3.14}$$

Since the variable v_2 has no immediate physical significance, we seek weighted combinations of the equations to eliminate the explicit dependence on the variable.

We assume that the general weighting function, $f(u_2)$, vanishes at the outer edge of boundary layer ($\eta = \infty$ or $u_2 = 1$). By multiplying (3.12a) by $f(u_2)$ and adding to $\frac{df(u_2)}{du_2} \times$(3.12b) and integrating the transformed equation from zero to one, with respect to

u_2, we obtain (3.15a).

$$\frac{\partial}{\partial\phi}\int_0^1 f\frac{w_2}{\tau}du_2 = \sin\theta_b\left(l_5\int_0^1 f\frac{w_2}{\tau}du_2 - 1.5\int_0^1 f\frac{u_2}{\tau}du_2\right. \tag{3.15a}$$
$$\left. + l_2\int_0^1 \frac{df}{du_2}\frac{\partial\tau}{\partial u_2}du_2 - l_1\int_0^1 \frac{df}{du_2}u_2\frac{w_2}{\tau}du_2 + \int_0^1 \frac{df}{du_2}\frac{w_2^2}{\tau}du_2\right)$$

The integral of the sum of $w_2\times$(3.12a), $w_2\times\frac{df(u_2)}{du_2}\times$(3.12b), and $f(u_2)\times$(3.12c) is equal to (3.15b).

$$\frac{\partial}{\partial\phi}\int_0^1 f\frac{w_2^2}{\tau}du_2 = \sin\theta_b\left(l_7\int_0^1 f\frac{w_2^2}{\tau}du_2 - 2.5\int_0^1 fu_2\frac{w_2}{\tau}du_2\right. \tag{3.15b}$$
$$- l_1\int_0^1 \frac{df}{du_2}u_2\frac{w_2^2}{\tau}du_2 + \int_0^1 \frac{df}{du_2}\frac{w_2^3}{\tau}du_2 + l_{11}\int_0^1 f\frac{(1-s)}{\tau}du_2$$
$$+ l_8\int_0^1 f\frac{u_2^2}{\tau}du_2 + l_2\int_0^1 \frac{df}{du_2}w_2\frac{\partial\tau}{\partial u_2}du_2 + l_2\int_0^1 f\frac{\partial\tau}{\partial u_2}\frac{\partial w_2}{\partial u_2}du_2$$
$$\left. + l_2\int_0^1 f\tau\frac{\partial^2 w_2}{\partial^2 u_2}du_2\right)$$

The integral of the sum of $s\times$(3.12a), $s\times\frac{df(u_2)}{du_2}\times$(3.12b), and $f(u_2)\times$(3.12d) is equal to (3.15c).

$$\frac{\partial}{\partial\phi}\int_0^1 f\frac{sw_2}{\tau}du_2 = \sin\theta_b\left(l_5\int_0^1 f\frac{sw_2}{\tau}du_2 - 1.5\int_0^1 fu_2\frac{s}{\tau}du_2\right. \tag{3.15c}$$

$$-l_1\int_0^1 \frac{df}{du_2}u_2\frac{sw_2}{\tau}du_2+\int_0^1 \frac{df}{du_2}\frac{sw_2^2}{\tau}du_2+l_2\int_0^1 \frac{df}{du_2}s\frac{\partial\tau}{\partial u_2}du_2$$
$$+l_3\int_0^1 f\frac{\partial}{\partial u_2}(\tau\frac{\partial s}{\partial u_2})du_2+l_4\int_0^1 f\frac{\partial}{\partial u_2}(\tau u_2)du_2+l_4\int_0^1 f\frac{\partial}{\partial u_2}(\tau w_2\frac{\partial w_2}{\partial u_2})du_2\Bigg)$$

It is assumed that there is no surface injection. Therefore v, and hence v_2, is zero at the wall. Since v_2 and $f(u_2)$ are zero at the wall and the outer boundary layer edge, respectively, v_2 no longer appears explicitly in the equations.

Recall from chapter 2 that if linear interpolation is to be used in the finite element method, the derivatives within the integral must be less than second order. The application of integration by parts to (3.15a-c), and dropping the numbered subscripts, results in (3.16a-c); the Dorodnitsyn [29] boundary layer formulation for the inclined cone.

$$\frac{\partial}{\partial\phi}\int_0^1 f\frac{w}{\tau}du=\sin\theta_b\Bigg(l_5\int_0^1 f\frac{w}{\tau}du-1.5\int_0^1 uf\frac{1}{\tau}du \tag{3.16a}$$
$$+l_2\int_0^1 \frac{df}{du}\frac{\partial\tau}{\partial u}du-l_1\int_0^1 \frac{df}{du}u\frac{w}{\tau}du+\int_0^1 \frac{df}{du}\frac{w^2}{\tau}du\Bigg)$$

$$\frac{\partial}{\partial\phi}\int_0^1 f\frac{w^2}{\tau}du=\sin\theta_b\Bigg(l_7\int_0^1 f\frac{w^2}{\tau}du-2.5\int_0^1 fu\frac{w}{\tau}du \tag{3.16b}$$
$$+l_2\int_0^1 \frac{df}{du}\frac{\partial}{\partial u}(w\tau)du-2l_2\int_0^1 \frac{df}{du}\tau\frac{\partial w}{\partial u}du-l_1\int_0^1 \frac{df}{du}u\frac{w^2}{\tau}du$$
$$+\int_0^1 \frac{df}{du}\frac{w^3}{\tau}du+l_{11}\int_0^1 f\frac{1}{\tau}du-l_{11}\int_0^1 f\frac{s}{\tau}du$$

$$+ l_8 \int_0^1 f\frac{u^2}{\tau}du - l_2 f\tau\frac{\partial w}{\partial u}\bigg|_0\Bigg)$$

$$\frac{\partial}{\partial\phi}\int_0^1 f\frac{sw}{\tau}du = \sin\theta_b\left(l_5\int_0^1 f\frac{sw}{\tau}du - 1.5\int_0^1 fu\frac{s}{\tau}du\right. \tag{3.16c}$$

$$-(l_2+l_3)\int_0^1 \frac{df}{du}\tau\frac{\partial s}{\partial u}du - l_1\int_0^1 \frac{df}{du}u\frac{sw}{\tau}du + \int_0^1 \frac{df}{du}\frac{sw^2}{\tau}du$$

$$-l_4\int_0^1 \frac{df}{du}u\tau du - l_4\int_0^1 \frac{df}{du}\tau w\frac{\partial w}{\partial u}du + l_2\int_0^1 \frac{df}{du}\frac{\partial}{\partial u}(s\tau)du$$

$$\left. - l_3 f\tau\frac{\partial s}{\partial u}\bigg|_0\right)$$

The four partial differential equations describing three-dimensional, viscous, compressible boundary layer, with explicit dependence on curvature, (3.5a-d) have been converted into a system of three integral equations. The Dorodnitsyn formulation of the equations of motion offers some significant advantages over even the simplifications in equations (3.12a-d).

To start, the weak form of the equations are being solved. This should decrease the errors in calculation since they are being averaged out across the boundary layer. By using u as an independent variable across the boundary layer, the infinite domain of η has been replaced by a finite domain. The high gradient of the variables in y have been decreased significantly, which results in high resolution of the dependent variables near the wall. This is of particular importantance in turbulent flow. The use of u as an independent variable also allows a uniform grid to be employed that automatically follows the growth of the boundary layer. The variable v_2 does not appear explicitly in the equations and can be recovered later. The shear stress, τ, along the cone generator, is solved for directly and should be particularly accurate.

3.2.2. Initial Conditions

In order to solve the integral equation, initial values of the dependent variables must be known. These values can be determined at the windward ray of symmetry.

At $\phi = 0$:

$$w = 0 \tag{3.17}$$
$$\frac{\partial p_e}{\partial \phi} = 0$$
$$\frac{\partial u}{\partial \phi} = 0$$

Again neglecting the numbered subscripts, equations (3.16a) and (3.16c) reduce to the following algebraic relations.

$$\int_0^1 f\frac{1}{\tau}\frac{\partial w}{\partial \phi}du = \sin\theta_b\left(-1.5\int_0^1 uf\frac{1}{\tau}du + l_2\int_0^1 \frac{df}{du}\frac{\partial \tau}{\partial u}du\right) \tag{3.18a}$$

$$\int_0^1 f\frac{s}{\tau}\frac{\partial w}{\partial \phi}du = \sin\theta_b\left(-1.5\int_0^1 fu\frac{s}{\tau}du - (l_2+l_3)\int_0^1 \frac{df}{du}\tau\frac{\partial s}{\partial u}du\right. \tag{3.18c}$$
$$\left. - l_4\int_0^1 \frac{df}{du}u\tau du + l_2\int_0^1 \frac{df}{du}\frac{\partial}{\partial u}(s\tau)du - l_3 f\tau\frac{\partial s}{\partial u}\Big|_0\right)$$

Since the cross flow velocity w is zero, (3.16b) must be differentiated with respect to ϕ. This reduces to (3.18b) at the windward ray.

$$\int_0^1 f\frac{1}{\tau}\left(\frac{\partial w}{\partial \phi}\right)^2 du = \frac{\sin\theta_b}{2}\left(-2.5\int_0^1 uf\frac{1}{\tau}\frac{\partial w}{\partial \phi}du + l_2\int_0^1 \frac{df}{du}\frac{\partial}{\partial u}\left(\frac{\partial w}{\partial \phi}\tau\right)du\right. \tag{3.18b}$$

$$-2l_2\int_0^1 \frac{df}{du}\tau\frac{\partial}{\partial u}\left(\frac{\partial w}{\partial \phi}\right)du + l_9\int_0^1 f\frac{1}{\tau}du - l_9\int_0^1 f\frac{s}{\tau}du$$

$$+l_{10}\int_0^1 f\frac{u^2}{\tau}du - l_2 f\tau\frac{\partial}{\partial u}\left(\frac{\partial w}{\partial \phi}\right)\Bigg|_0\Bigg)$$

3.2.3. Boundary Conditions

For the equations of motion ($\phi \neq 0$) the following Dirichlet conditions hold.

At the cone wall:

$$w = 0$$

$$u = 0$$

$$s = s_w = 1 - \frac{T_w}{T_0}$$

At the outer edge of the boundary layer:

$$w = \frac{w_e}{u_e}$$

$$u = 1$$

$$s = 0$$

At $\phi = 0$ the same Dirichlet type boundary conditions of (3.16a-c) hold, with the following additions.

At the cone wall:

$$\frac{\partial w}{\partial \phi} = 0$$

At the B.L. edge:

$$\frac{\partial w}{\partial \phi} = \frac{1}{u_e}\frac{\partial w_e}{\partial \phi}$$

4. APPLICATION OF FINITE ELEMENTS

4.1. Equations of Motion

As was explained in chapter 2, to determine the nodal values in the finite element method, the general weighting function, f(u), must be replaced by a set of linearly independent functions $f_k(u)$ (for k = 1, ... , N).

For this problem the set $f_k(u)$ is written as:

$$f_k(u) = (1-u)^2 N_k(u), \tag{4.1}$$

where $N_k(u)$ is the linear interpolation function, at a particular node k. The term $(1-u)$ is introduced to satisfy the requirement that $f_k(u)$ equal zero at the outer edge of the boundary layer. The squaring of $(1-u)$ prevents singularities from appearing in the integrals when the dependent variables are given their finite element interpretation.

The trial solutions for the dependent variables w, τ , and s are shown. The group finite element formulation, described in reference [51], is used in making the trial solutions of the various combinations of dependent variables.

$$\frac{w}{\tau} = \frac{u}{(1-u)} \sum_j N_j b1_j \tag{4.2}$$

$$\frac{w^2}{\tau} = \frac{u^2}{(1-u)} \sum_j N_j b2_j$$

$$\frac{sw}{\tau} = \frac{u}{(1-u)} \sum_j N_j b3_j$$

$$w = u \sum_j N_j b4_j$$

$$\tau = (1-u)\sum_j N_j b5_j$$

$$s = \sum_j N_j b6_j$$

$$\frac{1}{\tau} = \frac{1}{(1-u)}\sum_j N_j b7_j$$

$$\frac{w^3}{\tau} = \frac{u^3}{(1-u)}\sum_j N_j b8_j$$

$$\frac{s}{\tau} = \frac{1}{(1-u)}\sum_j N_j b9_j$$

$$w\tau = u(1-u)\sum_j N_j b10_j$$

$$\frac{sw^2}{\tau} = \frac{u^2}{(1-u)}\sum_j N_j b11_j$$

$$s\tau = (1-u)\sum_j N_j b12_j$$

The simultaneous imposition of the particular analytic variation of u within each element on the variables prevents the exact interrelationships from being satisfied except at the nodes or in the limit $N \to \infty$. The use of u outside of the summation sign is to insure the correct behavior of the dependent variables without invalidating the interrelationships at the nodes on the boundaries.

Substituting the representations of (4.2) into equations (3.16a-c) gives

$$\sum_j C1_{kj}\frac{db1_j}{d\phi} = \sin\theta_b \left(l_5 \sum_j C1_{kj} b1_j - 1.5\sum_j C1_{kj} b7_j + \right. \qquad (4.3a)$$

$$l_2\sum_j C2_{kj}b5_j - l_1\sum_j C3_{kj}b1_j + \sum_j C3_{kj}b2_j\Bigg)$$

for k = 1, ... , N

$$\sum_j C4_{kj}\frac{db2_j}{d\phi} = \sin\theta_b\left(l_7\sum_j C4_{kj}b2_j - 2.5\sum_j C4_{kj}b1_j + \right. \tag{4.3b}$$

$$l_2\sum_j C5_{kj}b10_j - l_1\sum_j C7_{kj}b2_j + \sum_j C7_{kj}b8_j +$$

$$l_{11}\sum_j C8_{kj}b7_j - l_{11}\sum_j C8_{kj}b9_j + l_8\sum_j C4_{kj}b7_j -$$

$$2l_2\left(C10A_kb5_{k-1}b4_{k-1} + C10B_kb5_{k-1}b4_k + C10C_kb5_kb4_{k-1} + \right.$$

$$(C10D_k + C10E_k)b5_kb4_k + C10F_kb5_kb4_{k+1} +$$

$$\left.\left.C10G_kb5_{k+1}b4_k + C10H_kb5_{k+1}b4_{k+1}\right)\right)$$

for k = 2, ... , N

$$= \left(, \ldots , -l_2b5_1b4_1\right) \text{ for } k = 1$$

$$\sum_j C1_{kj}\frac{db3_j}{d\phi} = \sin\theta_b\left(l_5\sum_j C1_{kj}b3_j - 1.5\sum_j C1_{kj}b9_j - l_1\sum_j C3_{kj}b3_j + \right. \tag{4.3c}$$

$$\sum_j C3_{kj}b11_j - l_4\sum_j C9_{kj}b5_j + l_2\sum_j C2_{kj}b12_j -$$

$$(l_2 + l_3)\left(C11A_kb5_{k-1}b6_{k-1} + C11B_kb5_{k-1}b6_k + C11C_kb5_kb6_{k-1} + \right.$$

$$(C11D_k + C11E_k)b5_kb6_k + C11F_kb5_kb6_{k+1} + C11G_kb5_{k+1}b6_k +$$

$$\left.C11H_kb5_{k+1}b6_{k+1}\right)\Big) - l_4\left(C12A_kb10_{k-1}b4_{k-1} + C12B_kb10_{k-1}b4_k + C12C_kb10_kb4_{k-1} + \right.$$

$$(C12D_k + C12E_k)b10_kb4_k + C12F_kb10_kb4_{k+1} + C12G_kb10_{k+1}b4_k +$$

$$\left.\left.C12H_kb10_{k+1}b4_{k+1}\right)\right)$$

for k = 2, ... , N

$$= \left(, \ldots , -l_3b5_1\frac{(b6_2 - b6_1)}{\Delta u}\right) \text{ for } k = 1,$$

where $C1_{kj}$ through $C12H_k$ are found in appendix A. With the use of finite elements, the integral equations of (3.16a-c) have been transformed into a system of ordinary differential equations. The solution of $b1_j$, $b2_j$, and $b3_j$, can be solved by a variety of numerical methods.

4.2 Initial Conditions

The application of the finite element method to the integral equations governing the initial conditions (3.18a-c) is done in an identical manner. The trial solutions for the dependent variables are similar to those in equation (4.2).

$$\frac{1}{\tau}\frac{\partial w}{\partial \phi} = \frac{u}{(1-u)}\sum_j N_j Q1_j \tag{4.4}$$

$$\frac{1}{\tau}\left(\frac{\partial w}{\partial \phi}\right)^2 = \frac{u^2}{(1-u)}\sum_j N_j Q2_j$$

$$\frac{s}{\tau}\frac{\partial w}{\partial \phi} = \frac{u}{(1-u)}\sum_j N_j Q3_j$$

$$\frac{\partial w}{\partial \phi} = u\sum_j N_j Q4_j$$

$$\tau = (1-u)\sum_j N_j Q5_j$$

$$s = \sum_j N_j Q6_j$$

$$\frac{1}{\tau} = \frac{1}{(1-u)}\sum_j N_j Q7_j$$

$$\frac{1}{\tau}\left(\frac{\partial w}{\partial \phi}\right)^3 = \frac{u^3}{(1-u)}\sum_j N_j Q8_j$$

$$\frac{s}{\tau} = \frac{1}{(1-u)} \sum_j N_j Q9_j$$

$$\tau \frac{\partial w}{\partial \phi} = u(1-u) \sum_j N_j Q10_j$$

$$\frac{s}{\tau} \left(\frac{\partial w}{\partial \phi} \right)^2 = \frac{u^2}{(1-u)} \sum_j N_j Q11_j$$

$$s\tau = (1-u) \sum_j N_j Q12_j$$

The Galerkin finite element formulation of equations (3.18a-c) is as follows:

$$- \sum_j C1_{kj} Q1_j + \sin\theta_b \left(- 1.5 \sum_j C1_{kj} Q7_j + l_2 \sum_j C2_{kj} Q5_j \right) = 0 \qquad (4.5a)$$

for $k = 1, \ldots, N$

$$- \sum_j C4_{kj} Q2_j + \frac{\sin\theta_b}{2} \left(- 2.5 \sum_j C4_{kj} Q1_j + l_2 \sum_j C5_{kj} Q10_j - \right. \qquad (4.5b)$$

$$l_1 \sum_j C7_{kj} b2_j + \sum_j C7_{kj} b8_j + l_9 \sum_j C8_{kj} Q7_j$$

$$- l_9 \sum_j C8_{kj} Q9_j + l_{10} \sum_j C4_{kj} Q7_j$$

$$- 2l_2 \left(C10A_k Q5_{k-1} Q4_{k-1} + C10B_k Q5_{k-1} Q4_k + C10C_k Q5_k Q4_{k-1} + \right.$$

$$(C10D_k + C10E_k) Q5_k Q4_k + C10F_k Q5_k Q4_{k+1} +$$

$$\left. \left. C10G_k Q5_{k+1} Q4_k + C10H_k Q5_{k+1} Q4_{k+1} \right) \right) = 0$$

for $k = 2, \ldots, N$

$$\left(, \ldots , - l_2 Q5_1 Q4_1 \right) = 0 \text{ for } k = 1$$

$$-\sum_j C1_{kj}Q3_j + \sin\theta_b \left(-1.5\sum_j C1_{kj}Q9_j - l_4\sum_j C9_{kj}Q5_j + l_2\sum_j C2_{kj}Q12_j - \right. \tag{4.5c}$$

$$(l_2 + l_3)\left(C11A_kQ5_{k-1}Q6_{k-1} + C11B_kQ5_{k-1}Q6_k + C11C_kQ5_kQ6_{k-1} + \right.$$

$$(C11D_k + C11E_k)Q5_kQ6_k + C11F_kQ5_kQ6_{k+1} + C11G_kQ5_{k+1}Q6_k +$$

$$\left.\left. C11H_kQ5_{k+1}Q6_{k+1} \right) \right) = 0$$

$$\text{for } k = 2, \ldots, N$$

$$\left(, \ldots , -l_3Q5_1 \frac{(Q6_2 - Q6_1)}{\Delta u} \right) = 0 \text{ for } k = 1 ,$$

where $C1_{kj}$ through $C11H_k$ are the same used in the equations of motion (4.3a-c).

Notice that (4.5a-c) are essentially nonlinear algebraic equations in $Q1_j$, $Q2_j$, and $Q3_j$. The equations can be solved by an assortment of iterative methods.

4.3 Boundary Conditions

At the wall (u = 0):

$$w = 0$$

$$s = s_w$$

For $\phi = 0$ we have in addition:

$$\frac{\partial w}{\partial \phi} = 0$$

Which give the following nodal values:

$$b3_1 = s_w b1_1$$

$$Q3_1 = s_w Q1_1$$

Notice that since τ gives a Neumann and not a Dirichlet type of boundary condition, the value of τ at the surface is not required by either equations (4.3a-c) or (4.5a-c).

At the outer edge of the boundary layer (u = 1):

$$w = \frac{w_e}{u_e}$$

$$\tau = 0$$

$$s = 0$$

For $\phi = 0$, we have in addition:

$$\frac{\partial w}{\partial \phi} = \frac{\partial}{\partial \phi}\left(\frac{w_e}{u_e}\right) = \frac{1}{u_e}\frac{\partial w_e}{\partial \phi},$$

which give the following nodal values:

$$b2_N = \frac{w_e}{u_e} b1_N$$

$$b3_N = 0$$

$$Q2_N = \frac{1}{u_e}\frac{\partial w_e}{\partial \phi} Q1_N$$

$$Q3_N = 0$$

Again, please note that the value of τ at the boundary layer edge need not have been specified. However, if $(1-u)$ where not used in the representation of τ, the nodal value of $b5_N$ would have approached zero as the number of nodes increased ($N \rightarrow \infty$). This would

mean that $b2_N$ and $b1_N$ would have had to satisfy two conflicting relationships at $u = 1$ ($\frac{b2_N}{b1_N} = \frac{w_e}{u_e}$ and $\frac{b2_N}{b1_N^2} \rightarrow 0$).

5. SOLUTION OF EQUATIONS OF MOTION

In this section the steps taken to solve the governing equations numerically, are shown.

5.1 Initial Conditions

The set of ordinary differential equations of (4.3a-c) can be solved by a marching algorithm. However, any marching scheme considered will require the values of the nodes ($b1_j$, $b2_j$, $b3_j$) at some initial circumferential position, ε, to start. The first step in solving for these nodal values, is to solve the equations of motion at $\phi = 0$. The initial condition equations (4.5a-c), as mentioned earlier, are a system of 3N-3 nonlinear algebraic equations that must be solved iteratively to give the initial nodal values. The nonlinear equations are solved numerically by a quasi-Newton iterative scheme. This scheme requires a reasonable guess of the 3N-3 initial values to begin the process. This becomes rather difficult if an appreciable number of elements are to be considered.

An efficient method for the solution of the initial conditions is presented. Using a similarity transformation, the partial differential equations (3.12a-d) are reduced to a system of ordinary differential equations.

$$\frac{d^3f}{d\eta^3} = -\frac{1}{l_2}\left(\frac{3}{2}f + l_{12}g\right)\frac{d^2f}{d\eta^2} \tag{B.4a}$$

$$\frac{d^3g}{d\eta^3} = -\frac{1}{l_2}\left[\left(\frac{3}{2}f + l_{12}g\right)\frac{d^2g}{d\eta^2} - \frac{df}{d\eta}\frac{dg}{d\eta} - l_{12}\left(\frac{dg}{d\eta}\right)^2 + \frac{l_{10}}{l_{12}\sin\theta_b}\left(\frac{df}{d\eta}\right)^2 + \frac{l_9 s_w}{l_{12}\sin\theta_b}\Lambda + \frac{l_9(1-s_w)}{l_{12}\sin\theta_b}\right] \tag{B.4b}$$

$$\frac{d^2\Lambda}{d\eta^2} = \frac{Pr}{s_w l_2}\left[-s_w\left(\frac{3}{2}f + l_{12}g\right)\frac{d\Lambda}{d\eta} + \frac{l_4}{l_2}\frac{d^2f}{d\eta^2}\left(l_2\frac{d^2f}{d\eta^2} - \left(\frac{3}{2}f + l_{12}g\right)\frac{df}{d\eta}\right)\right], \tag{B.4c}$$

where

$$u = \frac{df}{d\eta} \qquad \frac{\partial w}{\partial \phi} = l_{12}\sin\theta_b \frac{dg}{d\eta} \tag{B.2}$$

$$s = s_w(1-\Lambda) \qquad v = -(\frac{3}{2}f + l_{12}g)$$

The boundary conditions are:

At $\eta = 0$:

$$\frac{df}{d\eta} = 0, \qquad f = 0$$

$$\frac{dg}{d\eta} = 0, \qquad g = 0$$

$$\Lambda = 0$$

At $\eta = \infty$:

$$\frac{df}{d\eta} = 1 \qquad \frac{dg}{d\eta} = 1$$

$$\Lambda = 1$$

The details of the transformation, which is similar to that used by Moore [18],[48] and Reshotko [49], are discussed in appendix B.

Equations (B.4a-c) represent a relatively straight forward two point boundary value problem. The solution requires that the correct values for $\frac{d^2f}{d\eta^2}$, $\frac{d^2g}{d\eta^2}$ and $\frac{d\Lambda}{d\eta}$ be found at the wall which will cause $\frac{df}{d\eta}$, $\frac{dg}{d\eta}$ and Λ to approach the value of 1 as η approaches infinity. The numerical scheme used in integration was a fourth order Runge-Kutta method with a step size of 0.01. Integration up to an η of 6, was found to be sufficient.

The dependent variables τ, $\frac{\partial w}{\partial \phi}$, and s are found from (B.2) at the values of u required by (4.5a-c). The nodal values of $Q1_j$,$Q2_j$, and $Q3_j$ are then determined from the finite element representations of the three variables (4.4). At the boundaries however, the nodes are determined as follows:

At u = 0 ($\eta = 0$):

$$Q1_1 = \frac{l_{12}\sin\theta_b \frac{d^2g}{d\eta^2}}{\left(\frac{d^2f}{d\eta^2}\right)^2}$$

$$Q2_1 = \frac{\left(l_{12}\sin\theta_b \frac{d^2g}{d\eta^2}\right)^2}{\left(\frac{d^2f}{d\eta^2}\right)^3}$$

$$Q3_1 = \frac{s_w l_{12}\sin\theta_b \frac{d^2g}{d\eta^2}}{\left(\frac{d^2f}{d\eta^2}\right)^2}$$

At u = 1 ($\eta = \infty$):

$$Q1_N = -l_2 \frac{l_{12}\sin\theta_b}{(\frac{3}{2}f + l_{12}g)}$$

$$Q2_N = -l_2 \frac{\left(l_{12}\sin\theta_b\right)^2}{(\frac{3}{2}f + l_{12}g)}$$

$$Q3_N = 0$$

These values are then used as the initial guesses for the quasi-Newton iteration. Convergence of the iteration method is quite rapid. As the number of nodes increases for the finite element formulation, the values at the nodes approach those values determined from the similarity equations. For an appreciable number of nodes ($N > 5$) the iteration process can be skipped all together and the values determined from the similarity equations alone.

The starting values for the equations of motion are determined as follows.

At some small angle ε measured from the windward ray:

$$w(\varepsilon) = \varepsilon \frac{\partial w}{\partial \phi}(0)$$

$$\tau(\varepsilon) = \tau(0)$$

$$s(\varepsilon) = s(0)$$

therefore

$$b1_j = \varepsilon Q1_j \tag{5.1}$$

$$b2_j = (\varepsilon)^2 Q2_j$$

$$b3_j = \varepsilon Q3_j$$

The value of ε to be used, must be small enough so that the approximations made for τ and s are valid. However ε should be large enough that the values of $b2_j$ do not approach the round off error of the machine. The value found to work well in this study was an ε of 1°.

5.2 Equations of Motion

The marching algorithm to be used in the solution follows the theta method, outlined in references [45] and [46], and discussed in chapter 2. The ordinary differential equations of (4.3a-c) are replaced by an implicit finite difference approximation in ϕ.

Equations (4.3a-c) are rewritten as:

$$\sum_{j}^{N} C1_{kj}\Delta b1_j^{n+1} = \Delta\phi \left[\beta D1_k^{n+1} + (1-\beta)D1_k^n\right] \tag{5.2a}$$

$$\sum_{j}^{N} C4_{kj}\Delta b2_j^{n+1} = \Delta\phi \left[\beta D2_k^{n+1} + (1-\beta)D2_k^n\right] \tag{5.2b}$$

$$\sum_{j}^{N} C1_{kj}\Delta b3_j^{n+1} = \Delta\phi \left[\beta D3_k^{n+1} + (1-\beta)D3_k^n\right] \tag{5.2c}$$

for k = 1, ... , N where

$$\Delta b1_j^{n+1} = b1_j^{n+1} - b1_j^n$$

$$\Delta b2_j^{n+1} = b2_j^{n+1} - b2_j^n$$

$$\Delta b3_j^{n+1} = b3_j^{n+1} - b3_j^n$$

$D1_k$, $D2_k$, and $D3_k$ are the right hand sides of equation (4.3a), (4.3b) and (4.3c), respectively. The superscript n denotes a particular circumferential position. Here, the parameter β ($0 \le \beta \le 1$) is introduced to control the degree of implicitness. The quanities $D1_k^{n+1}$, $D2_k^{n+1}$, and $D3_k^{n+1}$ are linearized by expansion about the known position ϕ^n [52].

$$D1_k^{n+1} = D1_k^n(\phi^{n+1}) + \left(\frac{\partial D1_k}{\partial b1_j}\right)^n \Delta b1_j^{n+1} + \left(\frac{\partial D1_k}{\partial b2_j}\right)^n \Delta b2_j^{n+1} + \left(\frac{\partial D1_k}{\partial b3_j}\right)^n \Delta b3_j^{n+1} \quad (5.3a)$$

$$D2_k^{n+1} = D2_k^n(\phi^{n+1}) + \left(\frac{\partial D2_k}{\partial b1_j}\right)^n \Delta b1_j^{n+1} + \left(\frac{\partial D2_k}{\partial b2_j}\right)^n \Delta b2_j^{n+1} + \left(\frac{\partial D2_k}{\partial b3_j}\right)^n \Delta b3_j^{n+1} \quad (5.3b)$$

$$D3_k^{n+1} = D3_k^n(\phi^{n+1}) + \left(\frac{\partial D3_k}{\partial b1_j}\right)^n \Delta b1_j^{n+1} + \left(\frac{\partial D3_k}{\partial b2_j}\right)^n \Delta b2_j^{n+1} + \left(\frac{\partial D3_k}{\partial b3_j}\right)^n \Delta b3_j^{n+1} \quad (5.3c)$$

The linearization is substituted into (5.2a-c) and results in the following system.

$$\sum_j^N \left[\left(C1_{kj} - \beta\Delta\phi \left(\frac{\partial D1_k}{\partial b1_j}\right)^n \right) \Delta b1_j^{n+1} - \beta\Delta\phi \left(\frac{\partial D1_k}{\partial b2_j}\right)^n \Delta b2_j^{n+1} - \beta\Delta\phi \left(\frac{\partial D1_k}{\partial b3_j}\right)^n \Delta b3_j^{n+1} \right] = \Delta\phi\, DD1_k \quad (5.4a)$$

$$\sum_j^N \left[-\beta\Delta\phi \left(\frac{\partial D2_k}{\partial b1_j}\right)^n \Delta b1_j^{n+1} + \left(C4_{kj} - \beta\Delta\phi \left(\frac{\partial D2_k}{\partial b2_j}\right)^n \right) \Delta b2_j^{n+1} - \beta\Delta\phi \left(\frac{\partial D2_k}{\partial b3_j}\right)^n \Delta b3_j^{n+1} \right] = \Delta\phi\, DD2_k \quad (5.4b)$$

$$\sum_j^N \left[-\beta\Delta\phi \left(\frac{\partial D3_k}{\partial b1_j}\right)^n \Delta b1_j^{n+1} - \beta\Delta\phi \left(\frac{\partial D3_k}{\partial b2_j}\right)^n \Delta b2_j^{n+1} + \left(C1_{kj} - \beta\Delta\phi \left(\frac{\partial D3_k}{\partial b3_j}\right)^n \right) \Delta b3_j^{n+1} \right] = \Delta\phi\, DD3_k \quad (5.4c)$$

$DD1_k^n$, $DD2_k^n$, and $DD3_k^n$ are $D1_k^n$, $D2_k^n$, and $D3_k^n$ respectively using the modified coefficients $lx_1, \ldots, lx_{12}$.

For example

$$lx_l = \beta l_l^{n+1} + (1-\beta) l_l^n$$

The arrays $\left(\frac{\partial D1_k}{\partial b1_j}\right)^n$, $\left(\frac{\partial D1_k}{\partial b2_j}\right)^n$, ... , are Jacobians. The integrals $C1_{kj}$, ... , $C12H_k$ are functions only of u and therefore need only be evaluated once. The integrands reduce to polynomials of various orders and can be solved to very high accuracy by Gaussian quadrature [44]. The highest order polynomial encountered is six and therefore quadrature of an order of no higher than three need be used to solve all of the integrals.

The equations (5.4a-c) can be lumped into a single matrix equation as shown.

$$\sum_{m=1}^{3N} LHS_{lm} \Delta b_m{}^{n+1} = RHS_l \qquad l = 1, \ldots, 3N \tag{5.5}$$

where

$$\Delta b_m{}^{n+1} = \Delta b1_j{}^{n+1}, \Delta b2_j{}^{n+1}, \Delta b3_j{}^{n+1} \qquad j = 1, \ldots, N$$

$$b_m = b1_j, b2_j, b3_j$$

The array LHS_{lm} is a sparse 3N×3N matrix and RHS_l is a 3N vector containing the vectors $\Delta\phi DD1_k^n$, $\Delta\phi DD2_k^n$, and $\Delta\phi DD3_k^n$ respectively.

The boundary conditions are as follows:

$$\Delta b_{2N}{}^{n+1} = l_l{}^{n+1} \Delta b_N{}^{n+1} + \left(l_l{}^{n+1} - l_l{}^n\right) b_N{}^n \tag{5.6}$$

$$\Delta b_{2N+1}{}^{n+1} = s_w \Delta b_N{}^{n+1}$$

$$\Delta b_{3N}{}^{n+1} = 0$$

By incorporating the boundary conditions into equation (5.5) through the use of Lagrange multipliers [27], the length of the vector RHS_l is increased by three. The array LHS_{lm} is now a $(3N+3)\times(3N+3)$ matrix.

Equation (5.5) is solved at each step using a general LU decomposition algorithm. Rather than iterate at a particular ϕ position, the method varies the step size $\Delta\phi$ to achieve the desired accuracy. Before computing the new solution $b_j^{n+1} = \Delta b_j^{n+1} + b_j^n$ the step-size is determined in the following manner. As long as the maximum value of the ratio, $\frac{\Delta b_j^{n+1}}{b_j^n}$, exceeds a preset constant the step-size is halved, if this step-size is greater than the preset minimum. If the maximum value of the ratio is less than one tenth of the preset constant, the step-size is increased by 50%, if this step-size is less than the preset maximum. Since no iteration is required to calculate the solution at each ϕ, and since only moderate effort is required for the solution of the implicit difference equation, considerable computational efficiency is achieved.

6. RESULTS

6.1 Convergence Properties

The convergence rates for finite element approximations of w, τ, and s are plotted in figures 4, 5, and 6. The ordinate is the measure of the average discrete L2 norm of the relative error. The error used is calculated in the following manner.

$$\text{error}(w) = \frac{\left(\sum_{j=2}^{N-1}\left(\frac{w_j}{w_{jex}} - 1\right)^2\right)^{1/2}}{(N-2)} \tag{6.1a}$$

$$\text{error}(\tau) = \frac{\left(\sum_{j=1}^{N-1}\left(\frac{\tau_j}{\tau_{jex}} - 1\right)^2\right)^{1/2}}{(N-1)} \tag{6.1b}$$

$$\text{error}(s) = \frac{\left(\sum_{j=2}^{N-1}\left(\frac{s_j}{s_{jex}} - 1\right)^2\right)^{1/2}}{(N-2)} \tag{6.1c}$$

Where w_{jex}, τ_{jex}, and s_{jex} are the exact values at the respective node.

In order to eliminate errors due to the discretization of ϕ, in the spatial convergence results, the convergence study was taken at the windward ray. Recall from chapter 5 and appendix B, that the windward equations can be represented by the three ordinary differential equations

$$\frac{d^3f}{d\eta^3} = -\frac{1}{l_2}\left(\frac{3}{2}f + l_{12}g\right)\frac{d^2f}{d\eta^2} \tag{B.4a}$$

$$\frac{d^3g}{d\eta^3} = -\frac{1}{l_2}\left[\left(\frac{3}{2}f + l_{12}g\right)\frac{d^2g}{d\eta^2} - \frac{df}{d\eta}\frac{dg}{d\eta} - l_{12}\left(\frac{dg}{d\eta}\right)^2 + \frac{l_{10}}{l_{12}\sin\theta_b}\left(\frac{df}{d\eta}\right)^2 + \frac{l_9 s_w}{l_{12}\sin\theta_b}\Lambda + \frac{l_9(1-s_w)}{l_{12}\sin\theta_b}\right] \tag{B.4b}$$

$$\frac{d^2\Lambda}{d\eta^2} = \frac{Pr}{s_w l_2}\left[-s_w\left(\frac{3}{2}f + l_{12}g\right)\frac{d\Lambda}{d\eta} + \frac{l_4}{l_2}\frac{d^2f}{d\eta^2}\left(l_2\frac{d^2f}{d\eta^2} - \left(\frac{3}{2}f + l_{12}g\right)\frac{df}{d\eta}\right)\right] \tag{B.4c}$$

A solution to these equations, for $\alpha = 10°$, were obtained using a fourth order Runge-Kutta scheme with $\Delta\eta = 0.01$. This solution is used as the exact values in the convergence results.

The theoretical global convergence rate for linear elements applied to a linear problem is first order. It was expected that since the cone problem involved highly nonlinear equations and the solution involved the simultaneous prescription of w, τ, and s at each node, that the convergence rate would be less than first order. This is seen for the variables s and τ. However, the variable w achieves almost second order convergence. The errors of w, τ, and s for crude grids are quite good. For example with only two elements s has an error of approximately 15%, w has 11% and τ has only 5%. For four elements the errors for s, w, and τ are 11%, 2%, and 3% respectively and for eight elements s,w, and τ are 6%, 1%, and 2% respectively. Therefore, even though the theoretically expected convergence rate is not achieved for s and τ, this is offset by the high accuracy on course grids. For the variable w the benefits of both high convergence and accuracy on course grids, are enjoyed.

6.2 Numerical Results

The results presented are for a sharp cone with a half angle of 15° at angles of attack of 5° and 10°. The fluid properties used are for air. The flow parameter are given below.

$$\theta_b = 15^\circ \tag{6.2}$$

$$Re_x = 5\times10^5$$

$$M_\infty = 7$$

$$Pr = 1$$

$$C = 0.922$$

$$p_\infty = 0.282$$

$$U_\infty = 2.333$$

$$\frac{T_w}{T_0} = 0.5$$

Only two elements ($\Delta u = 0.5$) were used in the calculations. Through numerical experimentation the value of 10^{-2} was used to ensure stability during ϕ marching. The step size ($\Delta\phi$) varied from 10^{-5} to 10^{-3}. This program was run in double precision and on a VAX 11/780 at the NASA Ames Research Center.

Figure 7 shows the distribution of the surface coefficient of friction (C_{fw}) with the circumferential position ϕ for $\alpha = 5^\circ$ and 10° respectively. The coefficient is defined below.

$$C_{fw} = \frac{\bar{\mu}\dfrac{\partial \bar{w}}{\partial \bar{y}}}{\frac{1}{2}\rho_\infty \bar{U}_\infty^{\,2}} = C\frac{u_e}{U_\infty}\left(\frac{6p_\infty}{Re_x p_e}\right)^{1/2}\left(\tau\frac{\partial w}{\partial u}\right)_w \tag{6.3}$$

The influence of incidence on C_{fw} can be seen by comparing the curves of figure 7. For both angles of attack the C_{fw} varies smoothly from $\phi = 0^\circ$ reaching a maximum value at

approximately $\phi = 100°$ and falling off again toward zero as the leeward ray is approached. The values of C_{fw} for $\alpha = 10°$ are greater than that for $\alpha = 5°$ at all circumferential positions. The failure of C_{fw} to equal zero at $\phi = 180°$ for both angles of attack is probably caused by the buildup of interpolation errors, from the crude grid used (two elements), during marching.

Figure 8 shows the variation of the surface coefficient of friction in the radial direction (C_{fu}) with ϕ. The coefficient C_{fu} is defined as follows.

$$C_{fu} = \frac{\bar{\mu}\frac{\partial \bar{u}}{\partial \bar{y}}}{\frac{1}{2}\rho_\infty \overline{U_\infty}^2} = C\frac{u_e}{U_\infty}\left(\frac{6p_\infty}{Re_x p_e}\right)^{\frac{1}{2}}\left(\tau\right)_w \qquad (6.4)$$

As can be seen in the figure the maximum value of C_{fu} occurs at the windward ray ($\phi = 0°$) and falls smoothly to a nonzero value as ϕ approaches the leeward ray. The distribution of C_{fu} is dependent on how the velocity u_e and the thickness of the boundary layer varies circumferentially. For the test cases u_e increases with ϕ which would increase C_{fu}. However, the increase in boundary layer thickness, which decreases C_{fu}, overcomes the influence of u_e. The angle $\alpha = 10°$ is seen to give greater values of C_{fu} than $\alpha = 5°$ at $\phi = 0°$. This difference in values of C_{fu} decreases as ϕ advances. The decrease in difference seems to be a result of the insensitivity of the external conditions to incidence except in the windward region.

The relative heat transfer at the wall ($\frac{Q_w}{Q_{waxi}}$) is plotted, versus ϕ, in figure 9. The heat transfer is calculated in the following way.

$$\frac{Q_w}{Q_{waxi}} = \frac{\kappa \dfrac{\partial T}{\partial \bar{y}_w}}{\kappa \dfrac{\partial T}{\partial \bar{y}_{axi}}} = \frac{u_e}{u_{e_{axi}}} \left(\frac{p_{e_{axi}}}{p_e} \right)^{1/2} \left(\frac{\tau \dfrac{\partial s}{\partial u}}{\tau \dfrac{\partial s}{\partial u_{axi}}} \right)_w \tag{6.5}$$

The relative heat transfer seems to follow the same trends as the coefficient C_{fu}. As was seen for C_{fu} the maximum value of $\frac{Q_w}{Q_{waxi}}$ occurs at the windward ray and decreases smoothly as ϕ increases. Also, as was seen for C_{fu}, the effect of incidence is evident mostly in the windward region. These similar trends between heat transfer and C_{fu} were expected since the Prandtl number (Pr) was set equal to 1. The flow variable Pr = 1 makes the momentum and thermal boundary layers identical.

Figures 10 and 11 show the cross flow velocity profiles within the boundary layer at $\phi = 45°$, 90°, and 135°, for $\alpha = 5°$ and 10° respectively. The growth of the boundary layer with increasing ϕ is apparent. The profile curves are typical of three dimensional boundary layer flows, with a cross flow velocity maximum occuring within the layer [21]. Also, the influence of incidence on the profiles is noticable. As α increases from 5° to 10° the cross flow velocity increases, the velocity maximum shown at $\phi = 135°$ becomes more exaggerated, and the boundary layer increases in thickness.

The effects of incidence given are similar to the effects shown in references [1],[20],[21],[53].

7. CONCLUSIONS

7.1 Summary

A numerical method has been proposed to model the three-dimensional boundary layer about a yawed circular cone in a supersonic stream. It can, in principal, be extended to apply to the boundary layer of pointed bodies of arbitrary cross section.

The method reduces the three-dimensional boundary layer equations to two-dimensional form, through a coordinate transformation, and eliminates the explicit appearance of the normal velocity. The coordinate transformation also allows high resolution in the viscous region near the cone surface. The reduced boundary layer formulation is then presented in a Petrov-Galerkin finite element form and discretized across the layer using linear interpolation functions. Linear interpolation is the most computationally efficient to use from the family of piecewise continuous polynomials. The finite elements yield a system of ordinary differential equations in the circumferential coordinate. The system of differential equations, when put in a matrix form, yield a sparse mass matrix. The circumferential derivatives are then solved by a noniterative implicit marching scheme that gives both speed and stability. The results shown are in keeping with those given in previous studies. The proposed method gives acceptable accuracy with a very crude grid.

7.2 Future Work

Future applications of the finite element / finite difference method, by the author, will probably proceed as follows.

(i) The semidiscrete Galerkin modelling of the boundary layer about the cone will be linked with an interacting numerical model of the inviscid conical flow [24] for high angle of attack studies.

(ii) In a manner similar to that given by Holt [54]-[57], the boundary layer modelling will

also be carried on beyond flow separation into the reversed flow region and its reattachment.

(iii) The complete method will be applied to various cross sectional geometries.

REFERENCES

1. Helliwell, W.S. and Lubard, S.C. "An Implicit Method for Three-Dimensional Viscous Flow with Application to Cones at Angle of Attack," Aerospace Corp. Report TR-0074(4450-64)-1.

2. McRae, D.S. and Hussaini, M.Y. "Supersonic Viscous Flow over Cones at Incidence," Proceedings of the Sixth International Conference on Numerical Methods in Fluid Dynamics, p. 385-390, publ. as Lecture Notes in Physics, No. 90 (ed. M. Holt), Springer-Verlag (1978).

3. Degani, D. "Computation of Asymmetric Supersonic Flows Around Cones at Large Incidence," NASA-CR-180617, (1987).

4. Stone, A.H. "On Supersonic Flow Around a Slightly Yawed Cone," Part I, J. Math. and Phys. 27, 1, 67-81, (1948).

5. Stone, A.H. "On Supersonic Flow Around a Slightly Yawed Cone," Part II, J. Math. and Phys. 30, 200-213, (1952).

6. Van Tuyl, A.H. "Three-Dimensional Calculation of Vortices Behind a Missle at Large Angles of Attack," Boundary-Layer Effects-Proceedings of the 7th U.S. Air Force/FRG Data Exchange Agreement Meeting, AFFDL-TR-78-111,p. 340-349, (1958).

7. Wardlaw, A.B. Jr. "Multivortex Model of Asymmetric Shedding on Slender Bodies at High Angle of Attack," AIAA Paper 75-123, (1975).

8. Fletcher, C.A.J. "Supersonic Flow about Cones at Large Angles of Attack," Univ. of Calif., Berkeley, Fluid Mech. Rept. FM-74-8, (1974).

9. Kutler, P. and Lomax, H. "The Computation of Supersonic Flow Fields about Wing-Body Combinations by 'Shock-Capturing' Finite Difference Techniques," Proceeding of the Second International Conference on Numerical Methods in Fluid Dynamics, p. 24-29, publ. as Lecture Notes in Physics,

No. 8 (ed. M. Holt), Springer-Verlag, (1973).

10. Jameson, A., Schmidt, W. and Turkel, E., "Numerical Solutions of the Euler Equations by Finite Volume Methods Using Runge-Kutta Time Stepping Schemes," AIAA Paper 81-1259, June 1981.

11. Holt, M. and Blackie, J. "Experiments on Circular Cones at Yaw in Supersonic Flow," J. Aeronaut. Sci. 23, 10, 931-936, (1956).

12. Tracy, R.R. "Hypersonic Flow over a Yawed Circular Cone," Graduate Aero. Labs., Calif. Inst. of Technology, Pasadena, Calif., Memo. No. 69, (1963).

13. Rainbird, W.J. "The External Flow Field about Yawed Circular Cones," AGARD Conference Proceedings No. 30, Hypersonic Boundary Layers and Flow Fields, Paper No. 30, (1968).

14. Yahalom, R. "An Experimental Investigation of Supersonic Flow past Yawed Cone," Univ. of Calif., Berkeley, Aero. Sci. Rept. AS-71-2, (1971).

15. Bachmanova, N.S. and Lapygin, V.I. "Investigation of the Supersonic flow Around a Circular Cone at Large Angles of Attack," Iz. AN SSSR, MZhG, No. 6, 79-84, (1973).

16. Nebbeling, C. and Bannink, W.J. "Experimental Investigation of the Supersonic Flow Past a Slender Cone at High Incidence," J. Fluid Mech., 87, 3, 475-496, (1978).

17. Reda, D.C. "Boundary Layer Transition Experiments On Sharp, Slender Cones In Supersonic Free Flight," AIAA J. 17, 8, 803-810, (1979).

18. Moore, F.K. "Three-Dimensional Compressible Laminar Boundary-Layer Flow," NACA TN 2279, (1951).

19. Bashkin, V.A. Zh. Vychisl. Mat. Fiz. 8, 1280-1290, (1968).

20. Boericke, R.R. "Laminar Boundary Layer on a Cone at Incidence in Supersonic Flow," AIAA J. 9, 3, 462-468, (1971).

21. Dwyer, H.A. "Boundary Layer on a Hypersonic Sharp Cone at Small Angle of Attack," AIAA J. 9, 2, 277-284, (1971).

22. Marcillat, J. and Roux, B. AIAA J. 10, 1625-1630, (1972).

23. Lin, T.C. and Rubin, S.G. J. Fluid Mech. 59, 593-620, (1973).

24. Fletcher, C.A.J. and Holt, M. "Supersonic viscous flow over cones at large angles of attack," J. Fluid Mech. 74, 3, 561-591, (1976).

25. Finlayson, B.A. and Scriven L.E. "The Method of Weighted Residuals - A Review," Appl. Mech. Reviews, 19, 735-748, (1966).

26. Finlayson, B.A. *The Method of Weighted Residuals and Variational Principles*, Academic Press, (1972).

27. Chung, T.J. *Finite Element Analysis in Fluid Dynamics*, McGraw-Hill, (1978).

28. Fletcher, C.A.J. *Computational Galerkin Methods*, Springer-Verlag, (1983).

29. Dorodnitsyn, A.A. "General method of integral relations and its application to boundary layer theory," Adv. Aero. Sci. 3, 207-219, Pergamon,(1962).

30. Fletcher, C.A.J. and Fleet, R.W. "A Dorodnitsyn Finite Element Formulation for Laminar Boundary Layer Flow," Int. J. Num. Meth. Fluids 4,399-419, (1984).

31. Popinski, Z. and Baker, A.J. "An Implicit Finite-Element Algorithm for the Boundary Layer Equations," Jour. Comp. Phys., 21, 55-84, (1976).

32. Soliman, M.O. and Baker, A.J. "Accuracy and Convergence of a Finite Element Algorithm for Laminar Boundary Layer Flow," Comp. Fluids, 9, 43-62, (1981).

33. Baker, A.J. *Finite Element Computational Fluid Mechanics*, McGraw-Hill, (1983).

34. Carey, G.F. and Oden, J.T. *Finite Elements: Fluid Mechanics*, vol. VI, Prentice-Hall, (1986).

35. Davies, A.J. *The Finite Element Method: A First Approach*, Clarendon Press, (1980).

36. Dwoyer, D.L., Hussaini, M.Y. and Voigt, R.G. *Finite Elements Theory and Applications*, Springer-Verlag, (1988).

37. Mitchell, A.R. and Wait, R. *The Finite Element Method in Partial Differential Equations*, Wiley, (1977).

38. Segerlind, L.J. *Applied Finite Element Analysis*, Wiley, (1976).

39. Strang, G. and Fix, G.J. *An Analysis of the Finite Element Method*, Prentice-Hall, (1973).

40. Taylor, C. and Hughes, T.G. *Finite Element Programming of the Navier-Stokes Equations*, Pineridge Press Swansea, (1981).

41. Zienkiewicz, O.C. *The Finite Element Method*, 3rd ed., McGraw-Hill, (1977).

42. Anderssen, R.S. and Mitchell, A.R. "Analysis of Generalised Galerkin Methods in the Numerical Solution of Elliptic Equations," Math. Mech. Appl. Sci., 1, 3-15, (1979).

43. Galerkin, B.G. "Rods and Plates, Series Occurring in Various Questions Concerning the Elastic Equilibrium of Rods and Plates," (in Russian), Vestnik Inzhenerov, 19, 897-908, (1915).

44. Conte, S.D. and de Boor, C. *Elementary Numerical Analysis an algorithmic approach*, McGraw-Hill, (1972).

45. Richtmyer, R.D. and Morton, K.W. *Difference Methods for Initial-Value Problems*, Interscience, (1967).

46. Anderson, D.A., Tannehill, J.C. and Pletcher, R.H. *Computational Fluid Mechanics and Heat Transfer*, Hemisphere Publishing Corporation, (1984).

47. Golub, G.H. and Van Loan, C.F. *Matrix Computations*, John Hopkins, (1983).

48. Moore, F.K. "Laminar Boundary Layer on Cone in Supersonic Flow at Large Angle of Attack," NACA TR 1132, (1952).

49. Reshotko, E. "Laminar Boundary Layer with Heat Transfer on a Cone at Angle of Attack in a Supersonic Stream," NACA TN 4152, (1957).

50. Chapman, D.R. and Rubesin, M.W. "Temperature and Velocity Profiles in the Compressible Laminar Boundary Layer with Arbitrary Distribution of Surface Temperature," Jour. Aero. Sci., vol.16, no.9, pg.547-565, (1949).

51. Fletcher, C.A.J. "The Group Finite Element Formulation," Comp. Meth. Appl. Mech. Eng., 37, 225-243, (1982).

52. Briley, W.R. and McDonald, H. "Solution of the multi-dimensional compressible Navier-Stokes equations by a generated implicit method," J. Comp. Phys. 24, 372-397, (1977).

53. Feldhuhn, R.H., Winkelmann, A.E. and Pasiuk, L. "An Experimental Investigation of the Flowfield around a Yawed Cone," AIAA J. 9, 6, 1074-1081, (1971).

54. Holt, M. Proc. AGARD Conference on Separated Flows, p. 69-87, Rhode St. Genese, (1966).

55. Holt, M. Proc. XVII Int. Astronautical Congress, p. 383-401, Polish Scientific Publishers, (1967).

56. Holt, M. Proc. XVIII Int. Astronautical Congress, p. 385-397, Polish Scientific Publishers, (1968).

57. Holt, M., Lu, T.A. Acta Astronautica, 2, 409-429, (1975).

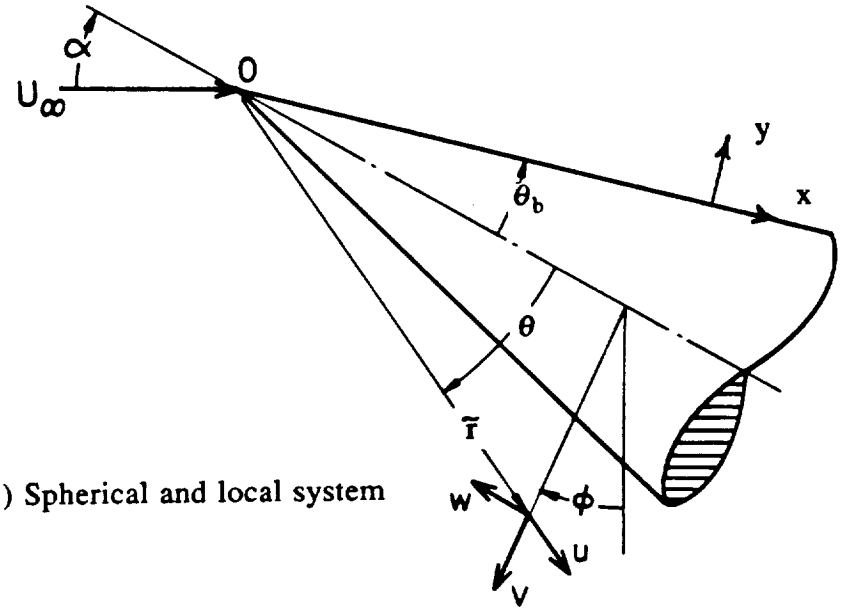

(a) Spherical and local system

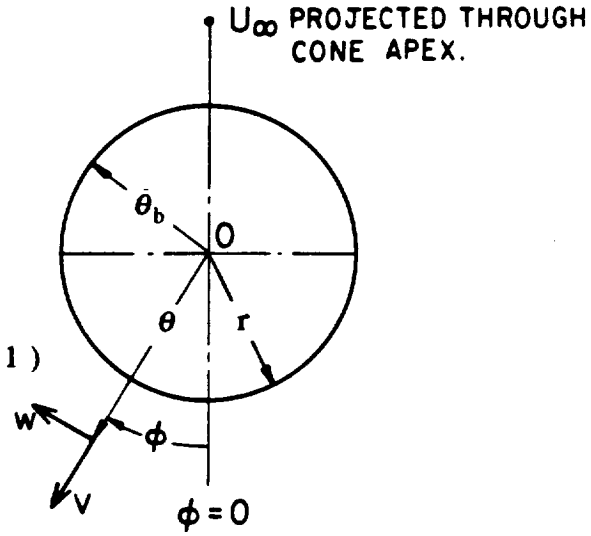

(b) ϕ - θ surface ($\tilde{r} = 1$)

Fig. 1. Coordinate system and velocity components.

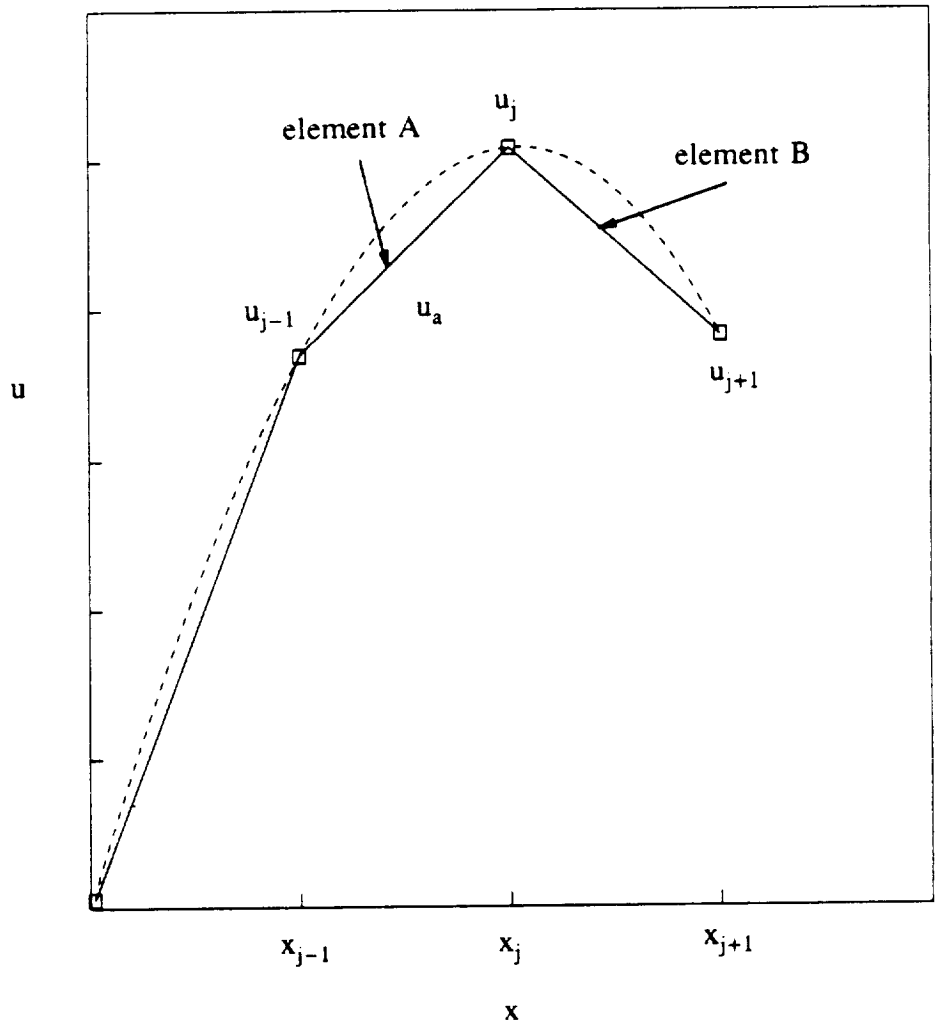

Fig. 2. Finite element representation using linear interpolation functions.

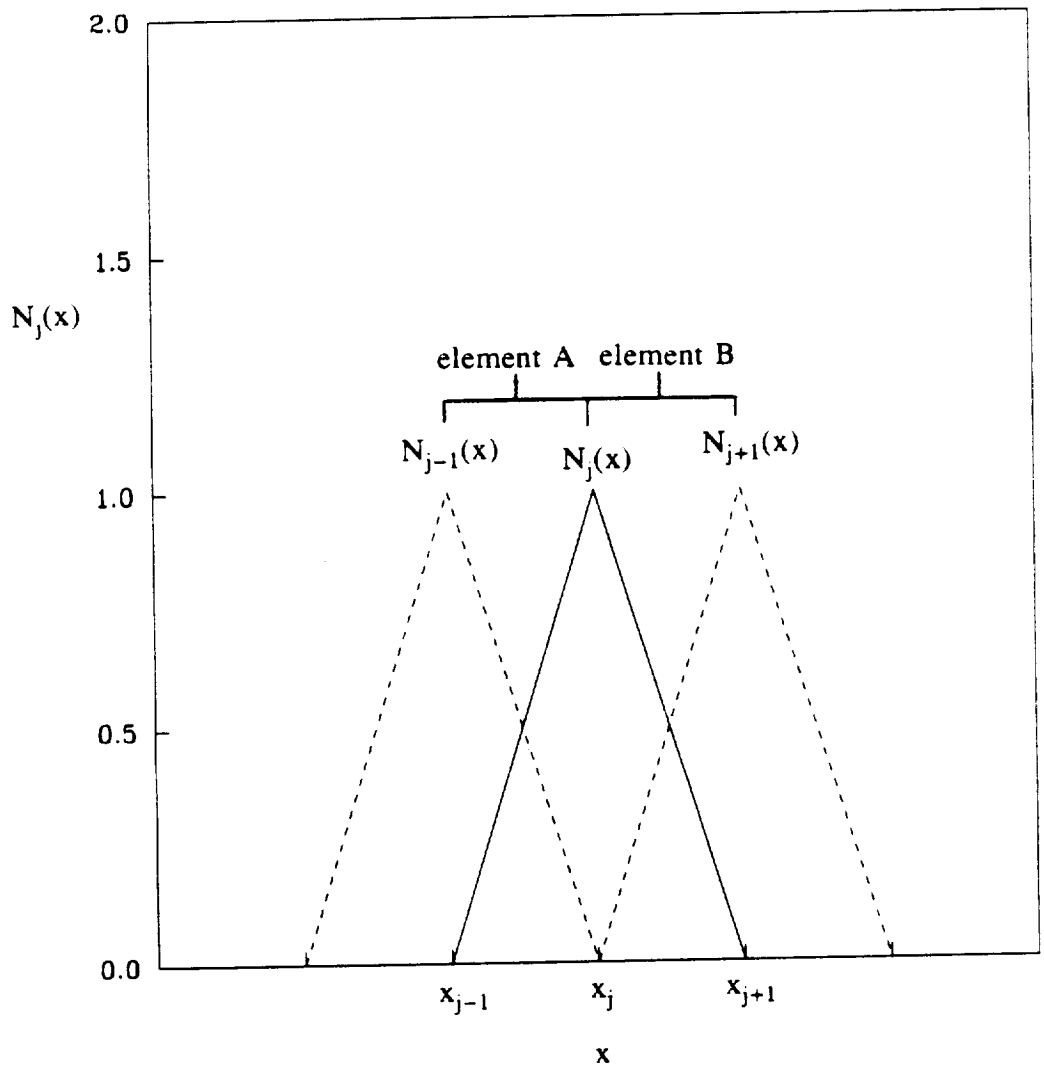

Fig. 3. Linear interpolation functions used in elements A and B of Fig. 2.

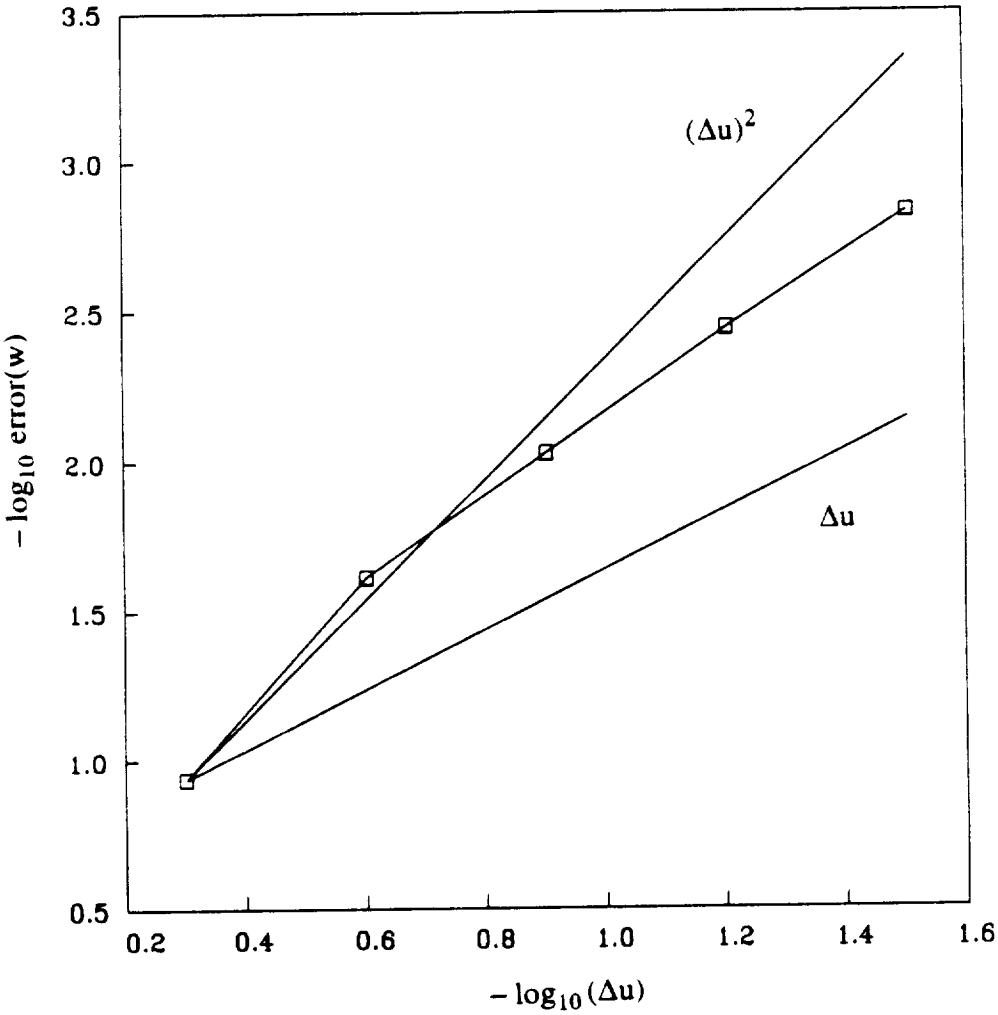

Fig. 4. Variation of the error in w with Δu.

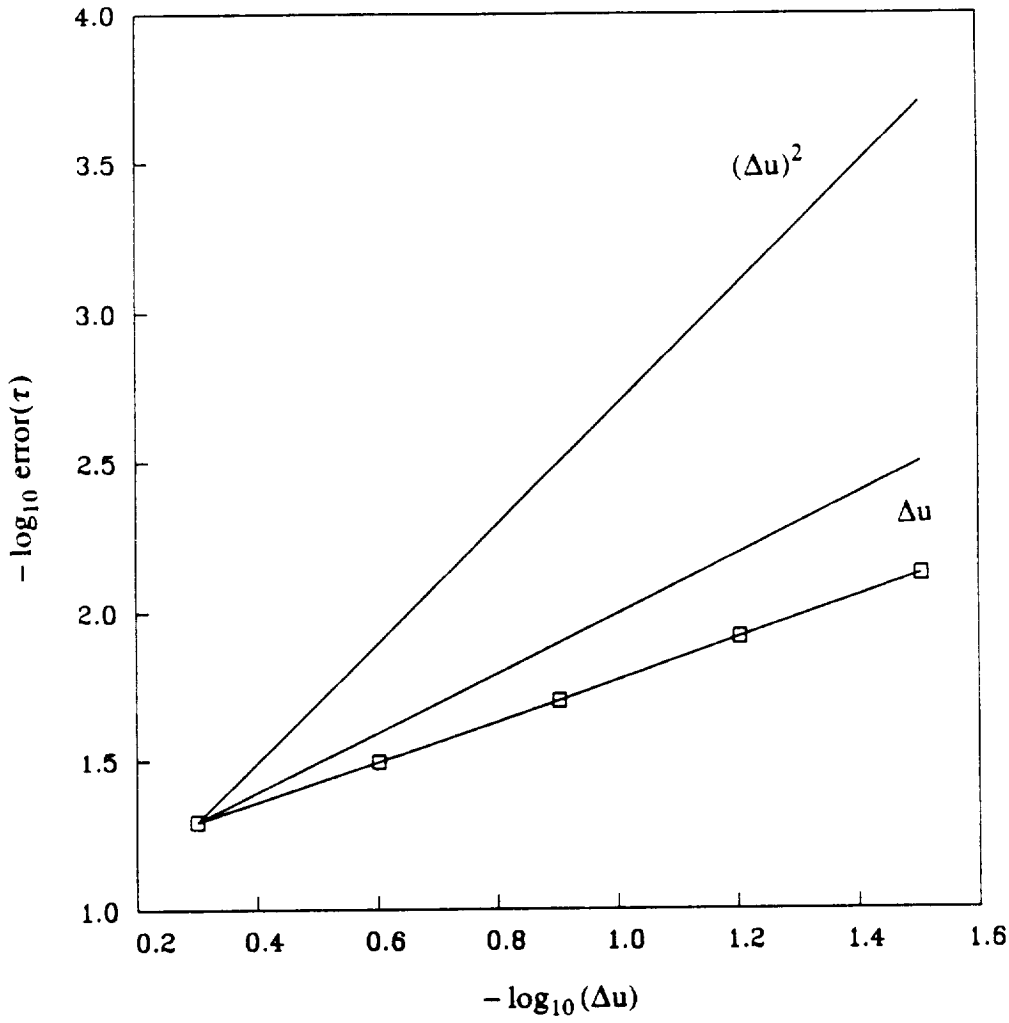

Fig. 5. Variation of the error in τ with Δu.

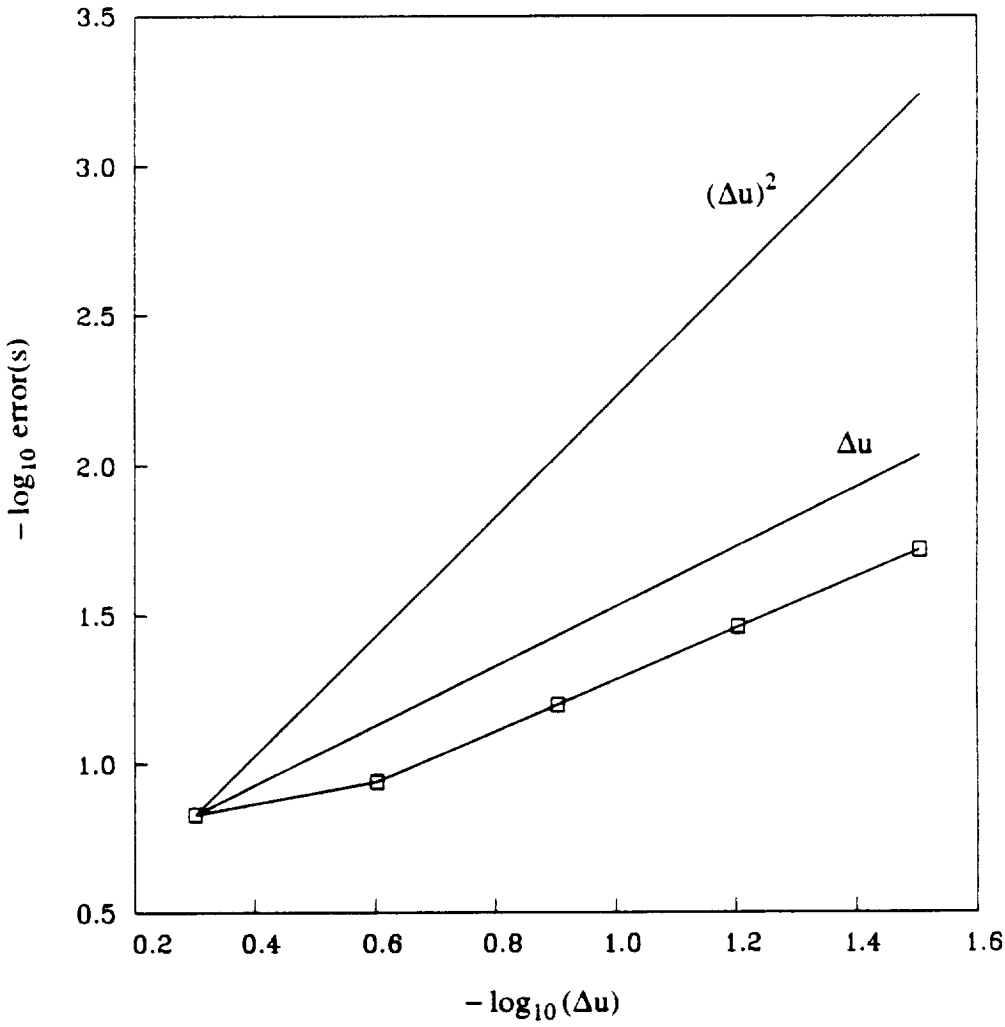

Fig. 6. Variation of the error in s with Δu.

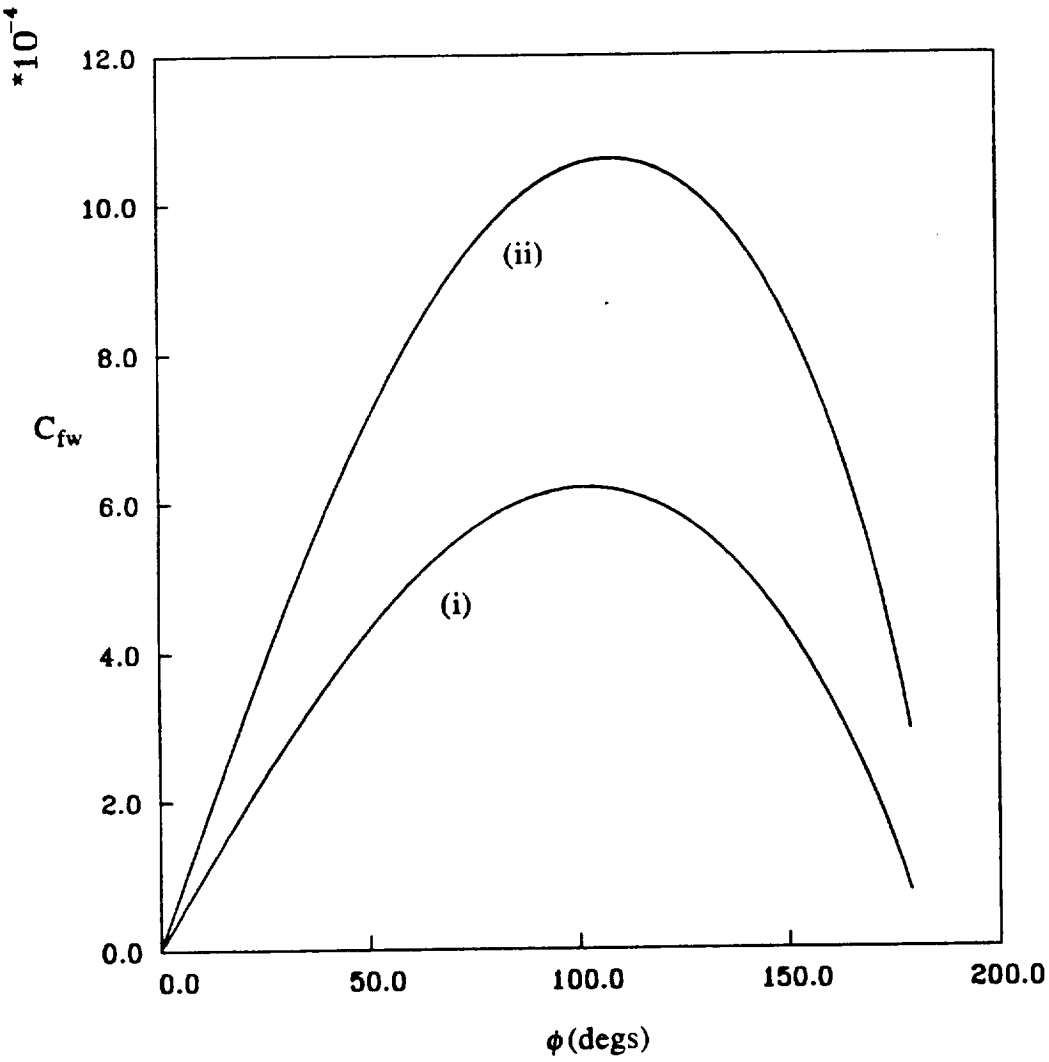

Fig. 7. Skin friction variation with incidence (ϕ component).

(i) $\alpha = 5°$. (ii) $\alpha = 10°$.

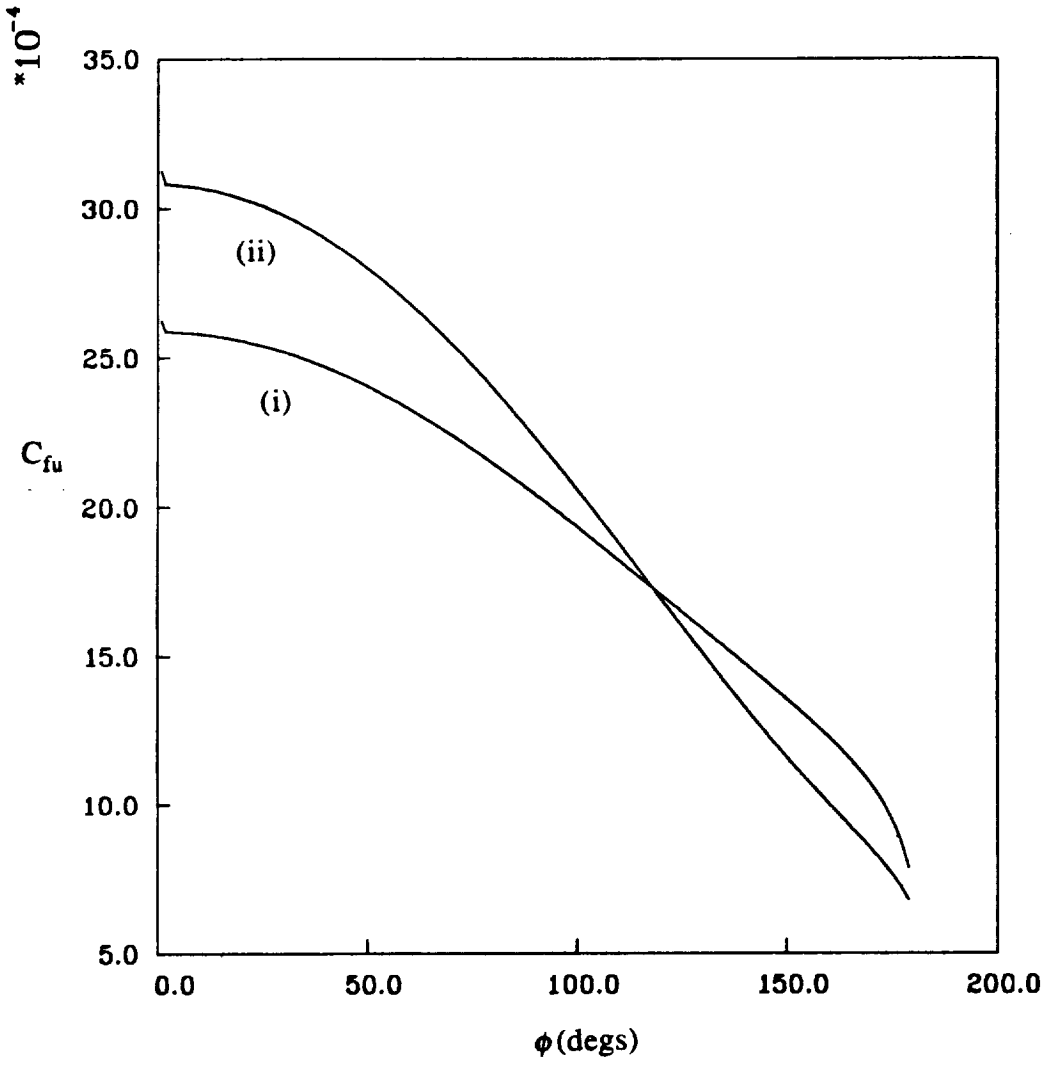

Fig. 8. Skin friction variation with incidence (x component).

(i) $\alpha = 5°$. (ii) $\alpha = 10°$.

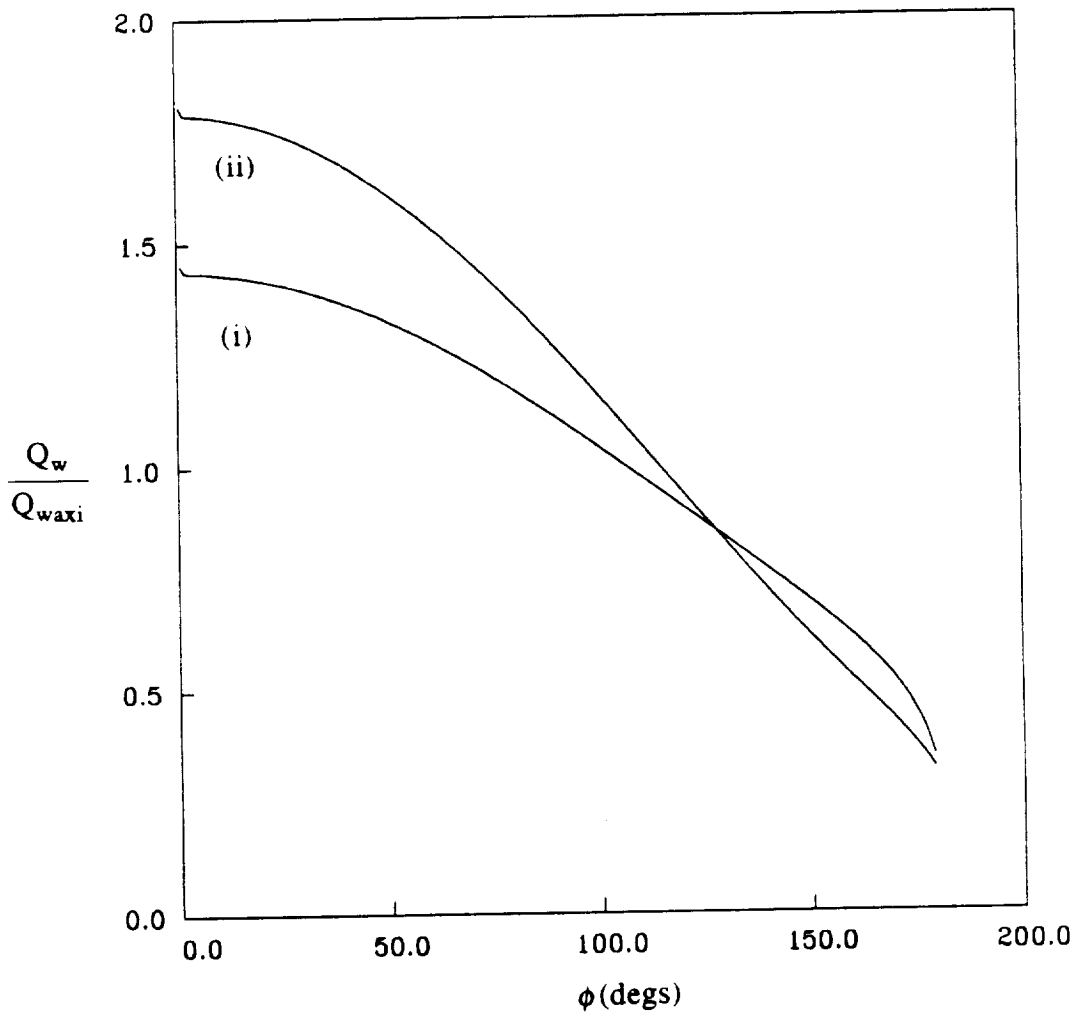

Fig. 9. Heat transfer variation with incidence.

(i) $\alpha = 5^{o}$. (ii) $\alpha = 10^{o}$.

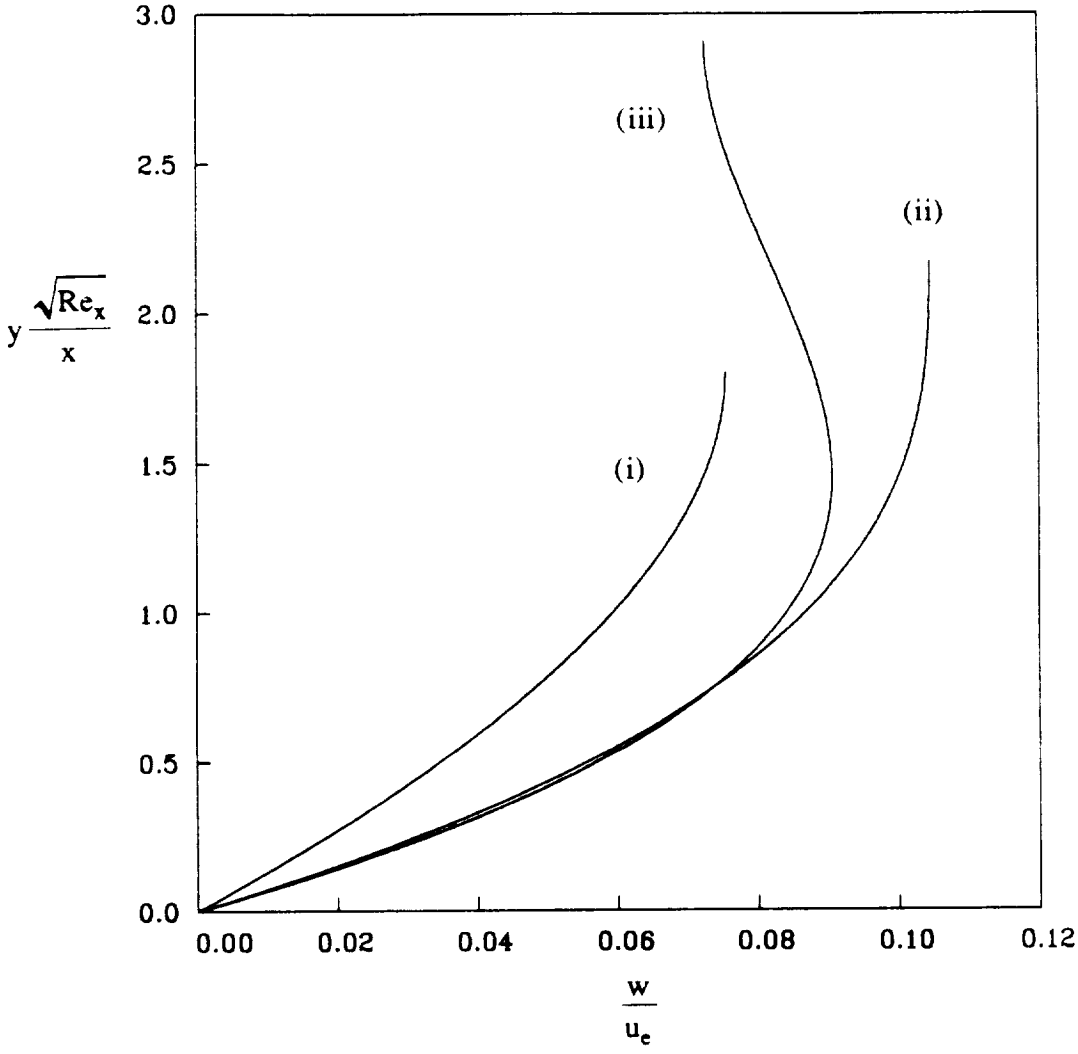

Fig. 10. Boundary layer profiles of the circumferential velocity component for $\alpha = 5°$.

(i) $\phi = 45°$. (ii) $\phi = 90°$. (iii) $\phi = 135°$.

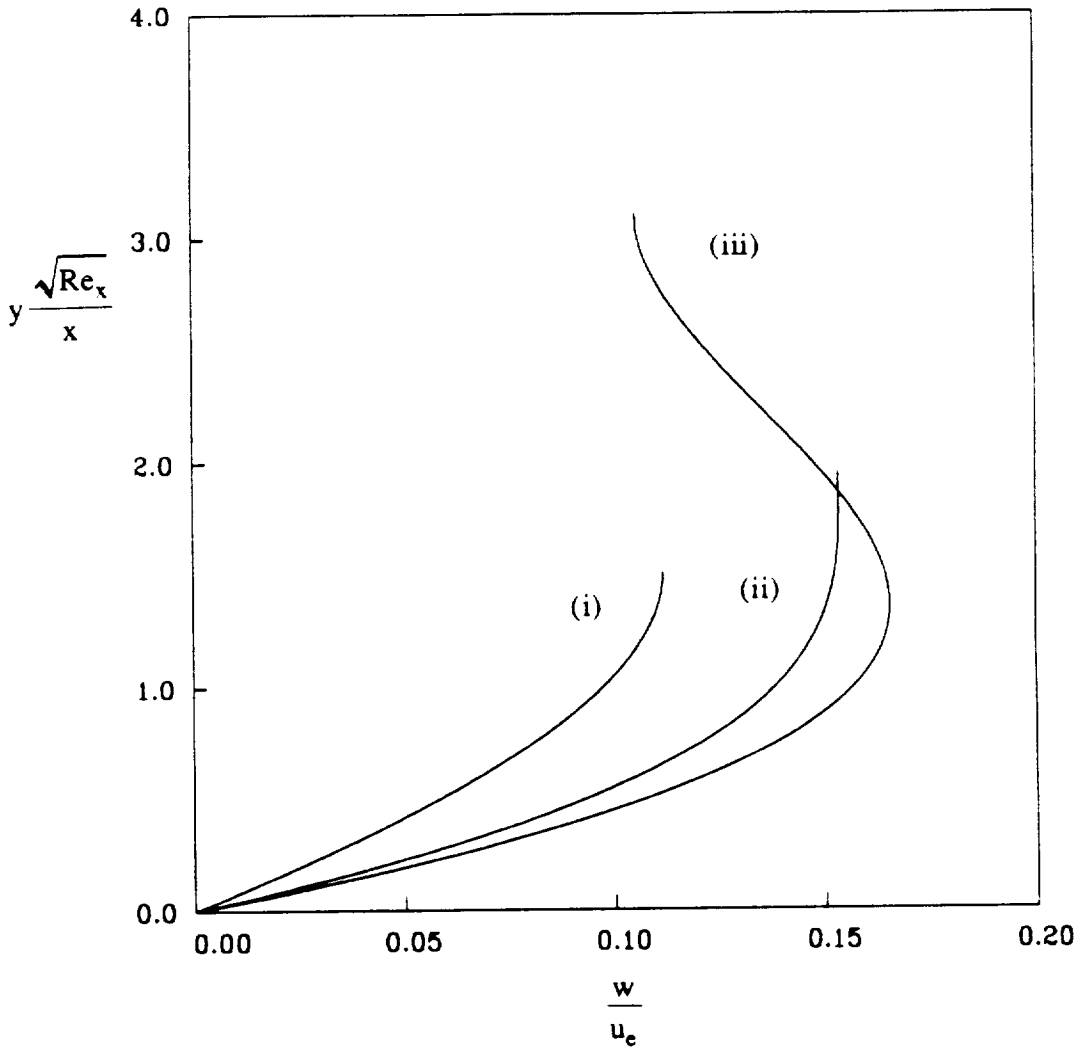

Fig. 11. Boundary layer profiles of the circumferential velocity component for $\alpha = 10°$.

(i) $\phi = 45°$. (ii) $\phi = 90°$. (iii) $\phi = 135°$.

APPENDIX A

A Definition of $C1_{kj}$ Through $C12H_k$

The components $C1_{kj}$ through $C12H_k$ first mentioned in chapter 3, are defined below.

$$C1_{kj} = \int_0^1 u(1-u)N_kN_j du$$

$$C2_{kj} = \int_0^1 (1-u)\left[(1-u)\frac{dN_k}{du} - 2N_k\right]\left[(1-u)\frac{dN_j}{du} - N_j\right] du$$

$$C3_{kj} = \int_0^1 u^2\left[(1-u)\frac{dN_k}{du} - 2N_k\right] N_j du$$

$$C4_{kj} = \int_0^1 u^2(1-u)N_kN_j du$$

$$C5_{kj} = \int_0^1 (1-u)\left[(1-u)\frac{dN_k}{du} - 2N_k\right]\left[u(1-u)\frac{dN_j}{du} + (1-2u)N_j\right] du$$

$$C6_{kj} = \int_0^1 (1-u)^2\left[(1-u)\frac{dN_k}{du} - 2N_k\right] N_j du$$

$$C7_{kj} = \int_0^1 u^3\left[(1-u)\frac{dN_k}{du} - 2N_k\right] N_j du$$

$$C8_{kj} = \int_0^1 (1-u)N_kN_j du$$

$$C9_{kj} = \int_0^1 u(1-u)^2\left[(1-u)\frac{dN_k}{du} - 2N_k\right] N_j du$$

$$C10A_k = \int_{u_{k-1}}^{u_k} (1-u)^2 \left[(1-u)\frac{dN_k}{du} - 2N_k\right] \left[u\frac{dN_{k-1}}{du} + N_{k-1}\right] N_{k-1}du$$

$$C10B_k = \int_{u_{k-1}}^{u_k} (1-u)^2 \left[(1-u)\frac{dN_k}{du} - 2N_k\right] \left[u\frac{dN_k}{du} + N_k\right] N_{k-1}du$$

$$C10C_k = \int_{u_{k-1}}^{u_k} (1-u)^2 \left[(1-u)\frac{dN_k}{du} - 2N_k\right] \left[u\frac{dN_{k-1}}{du} + N_{k-1}\right] N_k du$$

$$C10D_k = \int_{u_{k-1}}^{u_k} (1-u)^2 \left[(1-u)\frac{dN_k}{du} - 2N_k\right] \left[u\frac{dN_k}{du} + N_k\right] N_k du$$

$$C10E_k = \int_{u_k}^{u_{k+1}} (1-u)^2 \left[(1-u)\frac{dN_k}{du} - 2N_k\right] \left[u\frac{dN_k}{du} + N_k\right] N_k du$$

$$C10F_k = \int_{u_k}^{u_{k+1}} (1-u)^2 \left[(1-u)\frac{dN_k}{du} - 2N_k\right] \left[u\frac{dN_{k+1}}{du} + N_{k+1}\right] N_k du$$

$$C10G_k = \int_{u_k}^{u_{k+1}} (1-u)^2 \left[(1-u)\frac{dN_k}{du} - 2N_k\right] \left[u\frac{dN_k}{du} + N_k\right] N_{k+1}du$$

$$C10H_k = \int_{u_k}^{u_{k+1}} (1-u)^2 \left[(1-u)\frac{dN_k}{du} - 2N_k\right] \left[u\frac{dN_{k+1}}{du} + N_{k+1}\right] N_{k+1}du$$

$$C11A_k = \int_{u_{k-1}}^{u_k} (1-u)^2 \left[(1-u)\frac{dN_k}{du} - 2N_k\right] \frac{dN_{k-1}}{du} N_{k-1}du$$

$$C11B_k = \int_{u_{k-1}}^{u_k} (1-u)^2 \left[(1-u)\frac{dN_k}{du} - 2N_k\right] \frac{dN_k}{du} N_{k-1}du$$

$$C11C_k = \int_{u_{k-1}}^{u_k} (1-u)^2 \left[(1-u)\frac{dN_k}{du} - 2N_k\right] \frac{dN_{k-1}}{du} N_k du$$

$$C11D_k = \int_{u_{k-1}}^{u_k} (1-u)^2 \left[(1-u)\frac{dN_k}{du} - 2N_k\right] \frac{dN_k}{du} N_k du$$

$$C11E_k = \int_{u_k}^{u_{k+1}} (1-u)^2 \left[(1-u)\frac{dN_k}{du} - 2N_k\right] \frac{dN_k}{du} N_k du$$

$$C11F_k = \int_{u_k}^{u_{k+1}} (1-u)^2 \left[(1-u)\frac{dN_k}{du} - 2N_k\right] \frac{dN_{k+1}}{du} N_k du$$

$$C11G_k = \int_{u_k}^{u_{k+1}} (1-u)^2 \left[(1-u)\frac{dN_k}{du} - 2N_k\right] \frac{dN_k}{du} N_{k+1} du$$

$$C11H_k = \int_{u_k}^{u_{k+1}} (1-u)^2 \left[(1-u)\frac{dN_k}{du} - 2N_k\right] \frac{dN_{k+1}}{du} N_{k+1} du$$

$$C12A_k = \int_{u_{k-1}}^{u_k} u(1-u)^2 \left[(1-u)\frac{dN_k}{du} - 2N_k\right] \left[u\frac{dN_{k-1}}{du} + N_{k-1}\right] N_{k-1} du$$

$$C12B_k = \int_{u_{k-1}}^{u_k} u(1-u)^2 \left[(1-u)\frac{dN_k}{du} - 2N_k\right] \left[u\frac{dN_k}{du} + N_k\right] N_{k-1} du$$

$$C12C_k = \int_{u_{k-1}}^{u_k} u(1-u)^2 \left[(1-u)\frac{dN_k}{du} - 2N_k\right] \left[u\frac{dN_{k-1}}{du} + N_{k-1}\right] N_k du$$

$$C12D_k = \int_{u_{k-1}}^{u_k} u(1-u)^2 \left[(1-u)\frac{dN_k}{du} - 2N_k\right] \left[u\frac{dN_k}{du} + N_k\right] N_k du$$

$$C12E_k = \int_{u_k}^{u_{k+1}} u(1-u)^2 \left[(1-u)\frac{dN_k}{du} - 2N_k\right] \left[u\frac{dN_k}{du} + N_k\right] N_k du$$

$$C12F_k = \int_{u_k}^{u_{k+1}} u(1-u)^2 \left[(1-u)\frac{dN_k}{du} - 2N_k\right] \left[u\frac{dN_{k+1}}{du} + N_{k+1}\right] N_k du$$

$$C12G_k = \int_{u_k}^{u_{k+1}} u(1-u)^2 \left[(1-u)\frac{dN_k}{du} - 2N_k\right]\left[u\frac{dN_k}{du} + N_k\right] N_{k+1}du$$

$$C12H_k = \int_{u_k}^{u_{k+1}} u(1-u)^2 \left[(1-u)\frac{dN_k}{du} - 2N_k\right]\left[u\frac{dN_{k+1}}{du} + N_{k+1}\right] N_{k+1}du$$